Stable isotope evidence for near surface, low temperature formation of Mg-(hydro)carbonates in highly-altered Greek Mesozoic serpentinites

J.E. Andrews*[a], M.G. Stamatakis[b], I. Mitsis[b], T. Donnelly[c], M. Regueiro y González-Barros[d] and A.E. Fallick[c]

*corresponding author j.andrews@uea.ac.uk

Tel. +44 (0)1603 592536

[a]School of Environmental Sciences, University of East Anglia, Norwich, NR4 7TJ, UK

[b]Department of Geology & Geoenvironment, Section of Economic Geology & Geochemistry, National & Kapodistrian University of Athens, Panepistimiopolis, Ano Ilissia, 157 84 Athens, Greece

[c]Isotope Geosciences Unit Scottish Universities Environmental Research Centre East Kilbride, G75 0QF, Scotland.

[d]Instituto Geológico y Minero de España(IGME), Rios Rosas 22, Madrid 28003, Spain

Abstract

Authigenic magnesite, hydromagnesite and huntite associated with intensely altered and serpentinized ophiolitic rocks in Attica (mainland Greece) occur predominantly as veinlets and nodules within a totally weathered former-serpentinite groundmass. Carbonate $\delta^{18}O$ values are consistent with post-geothermal fluid temperatures between 25-70 ˚C, but mostly between 25-30 ˚C, from a dominantly meteoric-sourced groundwater, indicating near-surface, low-temperature conditions. Despite the proximity of a volcanic centre with strong CO_2 flux, 75% of the carbon isotope data imply little or no incorporation of this CO_2 into the authigenic Mg-(hydro)carbonates. Indeed, many $\delta^{13}C$ values are more negative than soil-zone calcrete values, and in this setting Mg-(hydro)carbonate $\delta^{13}C$ below -6‰ VPDB probably indicate disequilibrium effects in alkaline groundwaters. Geothermal fluids and groundwaters were mainly routed through structural conduits. Some of the low temperature hydromagnesite subsequently dehydrated to magnesite under near-surface conditions, while huntite is likely a diagenetic transformation of hydromagnesite, forming close to the volcanic centre where fluid Mg/Ca ratios were low. The isotopic signatures are distinct from previously published Balkan-East Mediterranean magnesite data arrays but are consistent with many other ultramafic-associated magnesium carbonates worldwide; their association with likely fluid compositions provide important context for Mg-(hydro)carbonate formation as geothermal conditions cool to near surface temperatures.

Keywords: magnesite, hydromagnesite, stable isotopes, serpentinization, weathering, Greece

It has been known since the late 1960s (Barnes et al. 1967; Barnes & O'Neil 1969) that the weathering of serpentinized-peridotites, typically in ophiolite complexes, results in hyperalkaline groundwater that may react with atmospheric CO_2 resulting in rapid precipitation of carbonate minerals. In the last few decades, interest in natural mineral carbonation, either as surface travertines or subsurface veins, has been reinvigourated as a safe and long-term method to sequester CO_2 from the atmosphere (e.g. Cipolli et al. 2004; Kelemen & Matter 2008; Park & Fan 2004; Wilson et al. 2009). It has been estimated, for example, that 10^4 to 10^5 tons per year of atmospheric CO_2 are converted to carbonate minerals (mainly magnesite and dolomite) during weathering and low temperature alteration of peridotites in Oman (Kelemen & Matter 2008). Natural carbonation can be accelerated by drilling, fracturing, and injection of purified CO_2 at elevated temperatures and pressures, such as those encountered at shallow depth in the crust. In particular, maintaining a temperature of 80 ^oC optimizes CO_2 uptake for *in situ* carbonation (Kelemen & Matter 2008). Experimental acid leaching of serpentinites produces magnesium-rich solutions which, when carbonated by bubbling with CO_2, precipitate hydromagnesite at pH 9 (Teir et al. 2009) along with pyroaurite or coalingite in field tests (Okamoto et al. 2006). Hydromagnesite is both thermally stable (up to 300 ^oC) and quite insoluble in water, making it a candidate mineral for long-term storage of CO_2.

In parallel to the carbon-storage context and often stimulated by economic interest in magnesite for industrial end-uses, there has been growing consensus that most ultramafic-hosted magnesites form under near surface conditions with involvement of meteoric water (see recent overviews in Keleman et al. 2011; Oskierski et al. 2013; Quesnel et al. 2013, 2016). While 'low' (typically <60 $^{\circ}C$) temperatures of magnesite mineralization are often inferred (Keleman et al. 2011) - usually from oxygen isotope data - precise temperatures of carbonation are difficult to ascribe, partly because the parent fluid is often not well-constrained, and because the magnesite-water oxygen isotope fractionation factor is still not fully resolved (Chako & Deines 2008). The 'temperature issue' is beginning to be addressed using clumped isotopes (García del Real et al. 2016). Magnesite carbon isotope compositions below -12‰ are also problematic and have attracted quite diverse interpretations (as described recently by Oskierski et al. 2013).

In this context we have been studying authigenic hydromagnesite ($Mg_5(CO_3)_4(OH)_2 \cdot 4H_2O$), magnesite ($MgCO_3$) and huntite ($CaMg_3(CO_3)_4$) mineralization, present mainly as veins and nodules in ophiolitic rocks of the West Attica Peninsula, mainland Greece (Fig.1). The host rocks have not only been intensely altered and serpentinized (Stamatakis & Mitsis 2013), but in parts of the study area have also been affected by volcanic and post-volcanic activity. Moreover, the nodular Mg-(hydro)carbonate masses in particular, appear to have soil-zone characteristics, as has been described by others for magnesite (Schroll 2002; Eslami et al. 2015), hydromagnesite (Mupton & Thompson 1966) and huntite (Stanger & Neal 1994).

We use stable isotope geochemistry to help better interpret the potentially complex geological conditions under which these Mg-(hydro)carbonates formed. The isotopic compositions of hydrothermal- and sedimentary-related Mg-(hydro)carbonates have been well-studied in the Balkan-East Mediterranean region (e.g. Fallick et al. 1991; Brydie et al., 1993; Zedef et al. 2000) and specifically for parts of Greece (Gartzos 2004), providing a framework for interpretation. However, a feature of this study is our ability to constrain interpretations of the isotopic data with likely fluid geochemical and isotopic compositions, and geologically-related palaeosol carbonates, an attribute that is critical in constraining genetic models (García del Real et al. 2016).

Geological, tectonic and geothermal features

The study area is bounded by the towns of Alepochori- Schinos – Soussaki – Ag Theodoroi on the West Attica Peninsula (Fig. 1) comprising rocks of the Viotian and Pelagonian geotectonic zones. The ophiolites, outcropping mainly in the Gerania Mountains, comprise Middle to Upper Jurassic ultramafics, dominated by spinel lherzolites of Western Mediterranean type (Vakondios 1996); they are tectonized, mylonitized, serpentinized and accompanied by dunitic bodies and some gabbroic veins (Spiliadis 1965; Vakondios 1996). The ophiolites overlie Triassic-Jurassic limestones (excepting one localised outlier of Palaeozoic schists) and are covered by Neogene sedimentary rocks (Mettos et al. 1982, 1988;

Bornovas et al. 1984; Gaitanakis et al. 1985; Vakondios 1996; Kaplanis et al. 2013).

The study area is well known for its intense tectonic and seismic activity, being located at the eastern end of the active Corinth Graben (Stiros 1995 and references therein). Three main deformation phases, from Triassic to Eocene times are described by Kaplanis et al. (2013) with high temperature ophiolite deformation apparent in places (Vakondios 1996); plastic deformation is clear both in the field and in thin section. Petrologic fabrics include intense undulatory extinction, crystal elongation, tectonic twinning of olivine, bending of the twinned crystals and exsolution of clinopyroxene in orthopyroxene (Cassard 1980; Vakondios 1996).

The degree of serpentinization does not increase with depth; rather, alteration of the ophiolite is most intense close to the carbonate basement over which it was thrust as allochthonous nappes (Bornovas et al. 1984, Gaitanakis et al. 1985). In the centre of the main ophiolite body, the degree of serpentinization and tectonic deformation is relatively weak (Vakondios 1996). By contrast, rocks of the north coastline of the study area (Schinos to Alepochori; Fig. 1) show intense serpentinization associated with a tectonic mélange comprising blocks of limestone and ophiolite (Fig. 1b). On the NW edge of the Pisia thrust (Schinos area LS-1 and LS-2 Fig. 1) the ultramafics are a loose serpentinitic breccia completely weathered to Mg-clays and often wet from modern groundwater seepage. Similarly, at the east edge of the Gerania thrust the peridotites are intensely sheared, resulting in a mylonite amphibolitic sole that overlies 100 m of strongly sheared ophiolitic mélange (Kaplanis et al. 2013). High serpentinite content is thus recorded at both the top of the nappe pile and deeper down in the sole, a geometry that suggests fluid flow was localised in faulted and thrusted zones. .

To the east and south the ultramafic rocks are overlain by 1 km of Upper Neogene marlstones, claystones, sandstones, conglomerates and thin (<1 m thick) lignites (Marinos 1951; Papp & Steininger 1979; Bentham et al. 1991; Collier & Dart 1991). Geophysical, structural, geochronological and geomorphological data indicate that

the Psatha, East Alkyonides, Schinos and Pisia faults (Holocene-active normal faults in the north part of the study area, LS-1, Fig. 1) are still active structures (Leeder et al. 2005; Gawthorpe et al. 2017) that accumulated some 360 m of footwall relief over ~2.2 Ma (Leeder et al. 2008).

Soussaki volcanic system

The southern part of the study area (Crommyonia) is not only tectonically and seismically active, but has also suffered volcanic activity, constituting the NW end of the Aegean volcanic arc. The Soussaki geothermal field (star symbol on Fig. 1), has locally altered ultramafics in the Soussaki and Agia Marina regions (LS-6, 7 and 8 on Fig. 1) and probably originates from volcanic intrusion into carbonate rocks at depth; a wide zone of rock has also been heated to around 225 ^{o}C by conduction (Demange & Gauthier 1992). Small outcrops of dacitic rocks are remnants of late-Pliocene to Quaternary (4.0-2.3 Ma) volcanic activity (Fytikas et al. 1986; Pe-Piper & Hatzipanagiotou 1997). The fluids localized in the ophiolites mainly come from a reservoir in limestones and dolomites at 900-1080 m depth (Vrellis et al. 1991). Borehole fluids have a mean temperature of 70 ^{o}C (Anonymous 1999) and are enriched in CO_2 and Ca^{2+} from reaction with host carbonates (Demange & Gauthier 1992). Today, post-volcanic activity is restricted to argillization processes, hydrothermal alteration-mineralization, acid leaching (acid rock drainage), fumaroles and thermal waters (Dotsika et al. 2009). In places, a weak mineralization of vein-stockwork magnesite is evident, having been commercially exploited on a small scale before 1939 (sites at Metalleion, Mnimata (LS-5 on Fig.1); authigenic minerals, mainly sulphates from volcanic emanations, are also present (Kyriakopoulos et al. 1990).

From late Pliocene times through to the present day,, extensional tectonic activity and sea-level changes have impacted the hydrological system causing leakage at the intersection of E-W and NW-SE trending faults, which allowed connection between the various geothermal reservoirs, regional groundwater and the surface. The ophiolite-hosted groundwater in the southern part of the study area is thus thought to consist of a deeply-sourced hot water mixed with descending meteoric water or ingressed seawater (see also isotope section). The hydrochemistry and

stable isotope values of thermal fluid samples collected from a 750 m deep well at Soussaki show a clear relationship with seawater (Dotsika et al. 2009). These hot waters have small enrichments in Cl^- and Na^+, a large enrichment in Ca^{2+}, K^+, Li^+, HCO_3^- and SiO_2 and depletion in SO_4^{2-} and Mg^{2+} with respect to local seawater, and are attributed to the interaction of seawater with rocks. δ^2H and $\delta^{18}O$ of the deep Soussaki well water are close to those of local seawater and indicate mixing between seawater and arc-type magmatic water (ATMW) with a large contribution from the former (Dotsika et al. 2009; Kelepertsis et al. 2001).

Gas emanations have CO_2 as the main component (>950 mmol/mol), and CH_4 and H_2S as minor components; the diffuse output of hydrothermal CO_2 from fumaroles and mofettes is about 630 gs^{-1} (54.4 Mgd^{-1}) estimated for an area of 0.015 km^2 at Theiochoma (LS-8 on Fig. 1), while the focused output is about 26 gs^{-1} (2.2 Mgd^{-1}; D'Alessandro et al. 2006). The CO_2 has $\delta^{13}C$ values between -1 to -2‰ VPDB, suggesting a predominant source of CO_2 from decarbonation reactions in the limestones (D'Alessandro et al. 2005). The CO_2 interacts with the geothermal waters to generate acidity which in-turn promotes rock-water interaction with quantitative leaching of cations and re-equilibration reactions (cf. Panichi et al. 2000).

Sampling and analytical techniques

We collected 115 mineralogical samples and 11 groundwater samples from wells, springs and fountains; sample localities (LS) are marked on Fig. 1 and specific details are given in Tables 1-4. Only the hard, concretionary, massive, white magnesite could be identified with confidence in the field; all other occurrences required powder X-ray diffraction (XRD) to confirm mineralogy. The XRD was a Bruker Model 5005 operated using Cu Kα radiation at 40 kV and 40 mA with 0.020° or 0.010° step size and 1.0 to 3.0 sec. step time. Mineral identifications were made with the EVA 10.0 Bruker DIFFRACplus software. In addition microfabrics were studied with a JEOL JSM-5600 scanning electron microscope (SEM) and an OXFORD LINK ISIS 300EDS electron probe microanalyzer (EPMA) was used for semi-quantitative elemental analysis. The system was operated at 20KV, 0.5nA and 50 sec dead time.

Water chemistry (metals) was measured using atomic absorption spectroscopy (AAS - Perkin Elmer model 1100b) while anions and the other chemical analyses were measured with a HACH: DR 4000 spectrophotometer, digital titrator and conductivity-TDS meter.

Stable isotope analyses were made on 35 carbonate sub-samples. Powdered samples (100 mesh) were reacted under vacuum with 103 percent H_3PO_4 (specific gravity 1.92) at 100°C in a hot block. At least eighteen hours were allowed for the reaction. The resultant CO_2 was then purified in the extraction line by the standard procedure of McCrea (1950). The ratios of $^{18}O/^{16}O$ and $^{13}C/^{12}C$ of the samples were analyzed on a triple collector mass spectrometer (ISOGAS, SIRA-10). A 1σ precision of ±0.3‰ or better for both carbon and oxygen isotopes was usually realized, although minor isotopic heterogeneity cannot be ruled out for some samples; this does not affect the conclusions drawn later. During the acid (H_3PO_4)-carbonate reaction, the $\delta^{18}O$ value of the released CO_2 is not the precise representative of the original carbonate mineral. For this reason $\delta^{18}O$ values must be obtained by using the oxygen isotope fractionation factor ($10^3 \ln \alpha$) which is specific for each mineral. For these magnesian carbonates we used a correction factor of 1.0093 (Rosenbaum & Sheppard 1986; see also Das Sharma et al. 2002). The hydromagnesite has been assigned the same factor as magnesite. The results are reported as delta values (δ‰) on the VSMOW and VPDB scales for oxygen and carbon respectively, and calibration of the laboratory working standard gas was via NBS 19 reacted at 25 °C.

The oxygen isotopic composition of water samples was measured using a modification of the 25 °C CO_2 equilibration method of Epstein & Mayeda (1953). In the automated gas interface linked to an AP 2003 mass spectrometer, 1 mL of each water was equilibrated with 300 μL of CO_2 (in He) in a 12 mL exetainer. The equilibrated CO_2 was dried and transferred by the He flow to the mass spectrometer for determination of $^{18}O/^{16}O$. The hydrogen isotopic composition of water samples was determined by the method of Donnelly et al. (2001) whereby 1μL aliquots were reduced to H_2 over chromium metal at 825 °C and the $^2H/^1H$ measured on an Optima or VG 602 mass spectrometer. Data are reported as δ‰ values relative to VSMOW and calibration was via international water standards. External precision and accuracy at 1σ were ±0.15‰ for $\delta^{18}O$ and ±2‰ for $\delta^{2}H$.

Results

Mg-(hydro)carbonate field relations and mineralogy

Mg-(hydro)carbonates are found mainly in the highly altered and sheared ultramafics close to the tectonic contact with Triassic carbonates (Fig. 1b) or in the regions affected by volcanic activity (Fig. 2a). Light microscopy shows network alteration in the earthy serpentinite host rocks, with relics of olivine, orthopyroxene, spinel, plagioclase, calcite and opaques. X-ray diffraction identified three Mg-(hydro)carbonates; magnesite, hydromagnesite and huntite, usually as single phases (Fig. 3 and Table 1) not mixed assemblages. In some samples, magnesite and huntite, or magnesite and hydromagnesite coexist, but never huntite and hydromagnesite.

In the field most Mg-(hydro)carbonates appear as veinlets or dispersed nodules in an earthy groundmass, some with a distinctive ‘cotton-ball’ morphology. Away from these areas only local vein magnesite mineralization was observed (Fig. 2b) and none of it has been deformed.

In the south of the study area (around Ag Theodoroi; Fig. 1), white nodular, botryoidal to nephroid accumulations of hard magnesite are common (Fig. 4a and b), while disseminated soft huntite nodules are rare. Scattered hydromagnesite nodules, up to 3 cm in diameter, occur in a distinct horizon immediately above the contact between the serpentinite and locally underlying Palaeozoic schists. Magnesite concretions are developed in a 10 m thick zone, above the hydromagnesite nodules, parallel to this contact.

In the south-central volcanic-affected area around Soussaki (LS-8), Ag Marina (LS-6) and Ag Dimitrios (LS-7; Fig. 1) hydromagnesite is common (Figs. 4c and d) with huntite only present in the close vicinity of volcanic/hydrothermal activity. The host rock here is an earthy serpentinite, with patchy silicification and hydrothermal staining. Nodules of huntite, up to 2 cm in diameter, are scattered throughout these highly altered rocks, and huntite is also present in boudinage layers up to 2 cm thick. Magnesite occurs mainly as layers of white nodules, crusts and cauliflower forms, some mm to several cm in thickness. Hydromagnesite cotton balls, up to 4 cm in

diameter (Figs 4c and d), and hydromagnesite fissure fillings are locally present (Figs 5a and b), sometimes close to huntite occurrences, but without any clear spatial or paragenetic association. Their association with faults (Fig. 4c) suggests the presence of 'diatreme-like' zones of alteration. In several hydromagnesite nodules a Mg-Fe-(Ni-rich) hydroxyl- carbonate type mineral of the pyroaurite group ($Mg_6Fe^{+3}_2(CO_3)(OH)_{16}\cdot 4H_2O$) occurs (Table 2).

In the north of the study area, the totally altered/weathered ultramafics (LS-1 and LS-2, Fig. 1) contain a horizon of disseminated hydromagnesite cotton balls >10 m thick (Fig. 6a) and near Schinos they can comprise almost 30% of the rock mass (Fig. 6b). The cotton balls range from millimeter to about 2 cm diameter (Fig. 6c; exceptionally up to ~5 cm diameter). Light microscopy reveals mainly serpentine with accessory minerals, calcite, talc, muscovite, plagioclase and opaques. At some outcrops, hydromagnesite also forms a highly friable network of fissure filling veinlets and crusts, resembling 'micro-stockwork' (Fig. 6d). In places where shear deformation occurred the cotton-balls and/or massive hydromagnesite stringers, with subordinate pyroaurite, form a honey-comb that rims rounded hard blocks of unaltered or altered serpentinite, 'floating' in the earthy groundmass (Figs 6a and b; cf. Mupton & Thompson 1966; De Wit et al. 1977; Chidester et al. 1978; Norrell et al. 1989). Tension cracks are also filled by hydromagnesite and in some places they have been disturbed by neotectonic action forming micro-faults in the fillings. Hard 'lettuce-leaf' magnesites are developed near the present-day ground surfaces in intensely altered earthy-clay (formerly ultramafics) of greenish or yellowish-brown colour; these lettuce-leaf magnesites occur above hydromagnesite cotton-ball accumulations (Figs 7a and b).

Microfabrics and elemental micro-analyses

Scanning electron microscopy shows that all the Mg-(hydro)carbonates are authigenic forming well-developed micro-crystals ranging from 0.5 to 20 μm. Typical chemical compositions from elemental microanalysis are shown in Table 2. Magnesite and huntite crystals are typically <2 μm in size (Figs. 3a and c), much smaller than the flakey hydromagnesite crystals that are >20 μm and exceptionally >200 μm (Figs 3b; see also Stamatakis 1995). Hydromagnesite may form pore

306 fillings on smaller, earlier formed hydromagnesite crystals and crystallinity is
307 typically best-developed where pore-filling euhedral hydromagnesite blades are
308 common (Figs 8a). Hydromagnesite frequently forms large aggregations with
309 pyroaurite, as well as serpentine, with pyroaurite crystals developing on
310 hydromagnesite blades (Fig. 8b). Magnesite may show colloform texture and there
311 is evidence of limited alteration to dolomite (Table 2) through a network of veinlets.
312

313 *Water chemistry and Mg/Ca ratio*

314 Chemical analysis of shallow surface spring waters (Table 3) from the highly altered
315 serpentinite in the north of the study area, close to the contact with the limestone,
316 show pH values >8.6, magnesium content between 87-154 mg L^{-1}, calcium content
317 <3 mg L^{-1}, and bicarbonate content between 371-578 mg L^{-1}. Spring waters
318 emerging in the area between Schinos and Mavro Limni (LS-1, Fig. 1), where
319 hydromagnesite cotton-balls are particularly widespread, have pH values of 9 to 9.3,
320 Mg^{2+} of 87 to 89 mg L^{-1} and a molar Mg/Ca ratio ~180 (Table 3).

321 Deeper groundwater from the Soussaki volcanic region is a mixture of seawater and
322 a small component of meteoric/volcanic water (Dotsika et al. 2009; Kelepertsis et al.
323 2001). Element concentrations are thus related to the seawater source with
324 magnesium concentrations 120-377 mg L^{-1}, and calcium concentrations of 64-210
325 mg L^{-1}, (Kelepertsis et al. 2001) yielding a molar Mg/Ca ratio ~3.5. For further
326 comparison, streams precipitating tufa ($CaCO_3$) in the N Peloponnese (Table 3)
327 have much lower molar Mg/Ca ratios around 0.4.

328

329 *Stable isotopes*

330 The Mg-(hydro)carbonates analyzed for stable isotopes were of two main types.

331 **Type 1:** 30 samples of near-surface cauliflower crusts, veinlets or nodular cotton
332 balls of magnesite, hydromagnesite or huntites, in altered earthy serpentinite. These
333 samples constitute the main focus of our study and are further subdivided in Table
334 1 into those within a few hundred metres of the moffettes and/or the associated
335 hydrothermal zones, and those further than a few hundred meters and up to 10 km
336 distant from obvious hydrothermal effects.

Type 2: Magnesite veins hosted in either ultramafic bedrock; (3 samples) or Neogene marl (2 samples). These samples were taken for comparison with Type 1.

These samples have a wide range of $\delta^{13}C$ values (-15.5 to +7.3‰) while $\delta^{18}O$ values are more constrained, mostly between +25 and +30‰. The data are shown in Table 1 and plotted on Figure 9. Where replicates or triplicates had significantly poorer reproducibility than analytical precision (Table 1), we infer likely natural heterogeneity. The isotopic compositions ($\delta^{2}H$ and $\delta^{18}O$) of water samples for the study area (springs, boreholes, seawater) are compiled in Table 3. Groundwater from springs and wells in the study area has $\delta^{18}O$ in the range -5.3 to -8.3‰. The water isotopic compositions mostly plot, as expected, close to the East Mediterranean Meteoric Water Line (Craig 1961). Samples from the Soussaki geothermal well have the isotopically heaviest compositions around -5.3‰, while those from the Gerania Mountains have a mean value of -7.4‰. A full discussion of local meteoric water $\delta^{2}H$ and $\delta^{18}O$ relationships is given in Dotsika et al. (2009) and the regional situation is described in Dotsika et al. (2010).

Discussion and Interpretations

Field appearance

The presence of Mg-(hydro)carbonate veinlets and nodules within a totally weathered former-serpentinite groundmass is a common attribute of near-surface, low temperature alteration of serpentinite bodies. The New Idria serpentinite of California (Mumpton & Thompson 1966) is a much cited ‘type example’ with O’Neil & Barnes (1971) describing the hydromagnesite there as ‘…clearly a weathering product of brucite and serpentinite.’ Our northern area sites in particular bear strong resemblance to New Idria in both appearance and mineralization. We also note that the predominantly nodular morphology of the Mg-(hydro)carbonates, particularly the ‘cotton-ball’ form, is similar to that of saline minerals such as ulexite that grow displacively in brine soaked mudflats (Smoot & Lowenstein 1991). In our study we interpret nodular growth to be similarly displacive in altered serpentinite groundmass which is more or less permanently wet, either below the groundwater table or in

zones of groundwater flow. Where volcanic and hydrothermal activity has affected the serpentinites the Mg-(hydro)carbonate mineralization is more complex (see above) but field relations are not fundamentally different, excepting the obvious hydrothermal staining, and the more brittle nature of the bedrock caused in part by patchy silicification. The lack of deformation in veins points to post compression tectonics mineralization.

Stable isotopes

While published data (e.g. Fallick et al. 1991; Brydie et al. 1993; Gartzos 2004; Zedef et al. 2000) on the isotopic composition of hydrothermal- and sedimentary-related Mg-(hydro)carbonates in Balkan-East Mediterranean region provide context we have interpreted our data from first principles in the framework of both known and likely fluid isotopic compositions and the most plausible paragenesis of the specific samples analysed. Where we have calculated equilibrium isotopic compositions for magnesite we have used the fractionation factor of Deines (2008) for carbon, and used the H_2O-magnesite oxygen isotope exchange of Aharon (1988) calibrated with dolomite data, partly as it has been widely used for cryptocrystalline magnesites, but also because García del Real et al. (2016) found it yielded realistic fluid compositions when using clumped isotope temperatures.

As outlined above, thermal fluids (60 - 75 ˚C) sampled at 750 m in the Soussaki borehole have $\delta^{18}O$ values ~+2‰ and $\delta^{2}H$ between +2.2 and +7.7‰ VSMOW, essentially seawater mixed with <10% Arc-Type Magmatic Water. CO_2 gas samples from this borehole and nearby Soussaki cave have $\delta^{13}C$ values of -1 to -2 ‰ VPDB consistent with CO_2 sourced from decarbonation of basement limestone. The field for magnesite precipitated in equilibrium with this fluid is marked on Figure 9. Near-surface well-waters in this region have $\delta^{18}O$ values ~ -5‰ and $\delta^{2}H$ ~ -32‰ (Table 3), less negative than the regional meteoric water described below and perhaps indicating a contribution from deep thermal waters.

Springs in the Gerania Mountains and in the north of the study area (Table 3) have $\delta^{18}O$ values of -6.4 to -8.3‰ (excepting one unusual value of -4.6‰ from a waterfall site). This range is consistent with the interpolated regional mean annual rainfall

400 $\delta^{18}O$ of ~-6 to -8‰ (OIPC v.2.2, Bowen & Revenaugh 2003) depending on elevation.
401 The groundwaters have temperatures ~20˚C and pH between 8 and 9 (Table 3),
402 typical of spring waters that have reacted with ultramafic rocks (e.g. Barnes & O'Neil
403 1969). HCO_3^- concentrations are high (350-600 mg L^{-1}); we have not measured the
404 $\delta^{13}C$ of the dissolved inorganic carbon (DIC; mainly HCO_3^- and CO_3^{2-} at these pH's),
405 but the range for ambient or mildly thermal waters in the Aegean region, including
406 ultramafic terrains, is between -8 and -15.5‰ (Gartzos 2004; Dotsika et al. 2009).
407 For context, fifty one modern-Late Pleistocene soil-zone calcretes in the nearby
408 Corinth and Megara Basins have a mean $\delta^{13}C$ of -8.7‰, the most negative value
409 being -10.2‰ (Table 4). In practice this implies that most soil-zone dominated DIC
410 in the study area is unlikely to have $\delta^{13}C$ much below -10‰. The field for Mg-
411 (hydro)carbonates precipitated in equilibrium with meteoric fluids of this type at 20
412 ˚C is marked on Figure 9. This predicted equilibrium field for magnesite is ~6‰ more
413 positive in $\delta^{18}O$ than the measured calcrete values, in good agreement with the
414 calcite-magnesite offset calculated by Chako & Deines (2008) at this temperature,
415 and as extrapolated from the data of Tarutani et al. (1969).

416

417 **Oxygen isotopes.** Mg-(hydro)carbonate $\delta^{18}O$ values >+28‰ (most of the data in
418 this study) can be explained as near equilibrium compositions from local meteoric
419 waters at temperatures between 25-30 ˚C (Fig. 9). Temperatures around 30 ˚C are
420 consistent with magnesite $\delta^{18}O$ inferred temperatures from many other studies (e.g.
421 Kadir et al. 2013; Kahya & Kuşcu 2014; Oskierski et al. 2012) including Quesnel et
422 al. (2016) and García del Real et al. (2017) where clumped isotopes were used to
423 help constrain temperatures. The remaining lower values probably result from mixed
424 fluids with temperatures above 40 ˚C, but we cannot be definitive about
425 temperatures, as mixed fluid compositions are not well-enough constrained.

426

427 **Carbon isotopes.** There is a clear grouping of Type 1 hydromagnesite and
428 magnesite samples that mostly come from the north of the study area (LS 1 and 2;
429 Fig. 1), furthest away from the volcanic centre. This is the area where the better-
430 formed cotton ball morphologies are found, and where groundwaters mostly have a
431 meteoric water signature (see above). These samples have negative $\delta^{13}C$ values

below -8‰. Magnesites with very negative $\delta^{13}C$ are not uncommon (e.g. Fallick et al. 1991; Zedef et al. 2000; Gartzos 2004; Kahya & Kuşcu 2014) and have typically been interpreted as resulting from isotopically light CO_2 sourced from thermally decomposing organic matter in metasediments inter-thrusted with ophiloite. However, in our study area there is no credible source of inter-thrust organic-rich metasediments. Thin lignites are present in some of the overlying Neogene sediments (Bentham et al. 1991; Collier & Dart 1991) but there is no evidence that they have either interacted with hydrothermal fluids, or have had any effective connectivity with the underlying aquifer.

Weathering-derived magnesites with $\delta^{13}C$ down to -13‰ have been interpreted as equilibrium values with soil-zone CO_2 derived from decomposition of plant organic matter (Jedrysek & Halas 1990; Oskierski et al. 2012). We think this unlikely in our case because local soil-zone calcretes (Table 4) do not have $\delta^{13}C$ below -10‰: equilibrium co-precipitated magnesites from these soil-waters at ~ 25 ˚C should not have $\delta^{13}C$ lower than about -4‰ using the fractionation offset of Deines (2008). As almost half of our (hydro)magnesite $\delta^{13}C$ values are much more negative than this, we interpret them as likely evidence for isotopic disequilibrium caused by the high groundwater pH.

When gaseous carbon dioxide interacts with alkaline aqueous fluid, a series of kinetic isotope fractionations occur, mainly favouring the light isotopes of carbon and oxygen which then can be preferentially incorporated into any carbonate precipitated. It is difficult to predict the expected carbonate $\delta^{13}C$ and $\delta^{18}O$ for geological samples because, as Usdowski & Hoefs (1986, 1988,1990) have shown, the kinetic fractionations are a function of the solution chemistry, its hydrodynamic properties, degassing history, and the evolution of its pH. Also, oxygen isotope exchange with the parental fluid can subsequently occur, bringing carbonate $\delta^{18}O$ back towards isotopic equilibrium with the fluid. Suffice here to note that if the CO_2 is predominantly atmospheric ($\delta^{13}C$ ~ -7‰) then carbonates with $\delta^{13}C \leq$ -15‰ are readily generated from alkaline (or once alkaline) solutions. Both field and experimental data show that travertine forming from calcium hydroxide spring water with pH >10.5 is influenced by uptake of atmospheric CO_2; the resulting isotopic fractionation yields $\delta^{18}O$ values ~7 to 12‰ more negative than equilibrium values, and $\delta^{13}C$ ~10 to 15‰ more negative than equilibrium values (O'Neil & Barnes 1971;

Clark et al. 1992; Fourcade et al. 2007). Moreover, there is limited field data (Andrews et al., 1997) suggesting these effects are still evident in waters with pH >9. The implied $\delta^{13}C$ shift in our lowest temperature (hydro)magnesite data is consistent with such disequilibrium (Fig. 9).

As the $\delta^{18}O$ values for this northern group (LS 1 and 2; Fig. 1) of Type 1 samples appear close to equilibrium it seems likely that decoupling between carbon and oxygen isotope fractionation occurred. For oxygen, isotope exchange with H_2O after kinetic fractionation, but before carbonate precipitation, would yield carbonate with a near-equilibrium composition, an effect not seen in carbon because there was no large pool of carbon to exchange with.

While we cannot be definitive regarding fractionation and re-equilibration, our data agree well with recent studies where a near-surface, low-temperature, meteoric-water origin for ultramafic-hosted magnesites has been proposed (Oskierski et al. 2012; Quesnel et al. 2013, 2016) and also in the classic work of O'Neil & Barnes (1971). Data fields from these studies are shown in Figure 9 for comparison with our values. Interestingly both the recent studies consider the possibility that disequilibrium effects, particularly for $\delta^{13}C$, are important; however, Oskierski et al. (2012) dismiss them as unlikely, while Quesnel et al. (2016) are equivocal about their role.

Most of the other Type 1 magnesites have $\delta^{13}C$ values typically between -6 and -2.5‰ (blue symbols, Fig. 9), compositions that are close to equilibrium with soil-zone CO_2 (Fig. 9). There is also a group of Type 1 samples, including all the huntites, collected close to the volcanic centre (orange symbols, Fig. 9) with $\delta^{13}C$ values between -4 and +2‰, again close to equilibrium with soil-zone CO_2. $\delta^{13}C$ values >0‰ probably incorporated CO_2 sourced from decarbonation /dissolution of basement limestone. Four samples, including the two Type 2 vein magnesites that intrude Neogene marls (Table 1), have $\delta^{13}C$ values between +4 and +7.3 ‰, and three of these have the lowest $\delta^{18}O$ values measured in the study. The isotopically enriched carbon values evoke a fluid with a large component of the thermal Soussaki fluid 'end-member' composition (Fig. 9), although the $\delta^{18}O$ values are not diagnostic: indeed, none of these samples are located close to the volcanic centre. A clumped isotope study is required to be more definitive on this issue.

Vein magnesites

The three Type 2 vein magnesites that intrude ultramafics have relatively constant isotopic composition with $\delta^{13}C$ values between -9.2‰ and -9.9‰ and $\delta^{18}O$ between +27.8‰ and +28‰. These values may represent an earlier phase of mineralisation, or possibly re-equilibration of original stockwork mineralization with younger mixed fluids. While these values are consistent with those described by Fallick et al. (1991) for Yugoslavian magnesite deposits, our proposed source of isotopically-light carbon is different, in accord with the geological context.

Paragenesis

The field relations and isotopic data point overall to a near-surface, low-temperature hydrothermal/weathering source for the Mg-(hydro)carbonate minerals. The hydrothermal signature may be pre- and/or co-genetic with weathering, and while we cannot constrain temperatures attained in the past, the isotope data show that most of the Mg-(hydro)carbonates in this study formed (or re-equilibrated) at temperatures at or below 30 ˚C. This interpretation, supported by similar recent field case studies (Oskierski et al. 2012; Quesnel et al. 2013, 2016) conflicts with earlier laboratory work (Hänchen et al. 2008; Möller 1989; Sayles & Fyfe 1973; Stevula et al. 1978) where magnesite does not precipitate until fluid temperatures are in the range 60-120 ˚C.

The volcanic centre in the south of the study area may have supplied geothermal CO_2 contained in hydrothermal fluids and gases that interacted with the ultramafic bedrock;

$$Mg_3Si_2O_5(OH)_4 + 3CO_2 + 2H_2O \rightarrow 3MgCO_3 + 2SiO_2 + 4H_2O.$$

although the isotopic record of temperatures >40 ˚C is very limited. This generic reaction does not capture the likely complexity of initial incongruent dissolution with an initial exchange of surface Mg^{2+} with H^+ on a brucite type surface (Stumm 1992), but the silicification observed in the vicinity of the volcanic centre is predicted. The spatial distribution of heavy alteration and carbonation in the

527 tectonically deformed zones implies later, normal-faulting-associated fracture-
528 controlled access for hydrothermal gases and fluids into domains in the
529 ultramafics. This normal faulting initiated in the late Pliocene (Gawthorpe et al.
530 2017).

531 The dissolution of residual olivine and orthopyroxene during low temperature
532 hydrothermal reaction or weathering would also promote both excess Mg^{2+} and
533 alkalinity to pore waters, both of which are important controls on the precipitation
534 of Mg-carbonates.

535 $Mg_2SiO_4 + 4H_2CO_3 \rightarrow 2Mg^{2+} + H_4SiO_4 + 4HCO_3^-$

536 $MgSiO_3 + 2H_2CO_3 \rightarrow Mg^{2+} + SiO_2 + 2HCO_3^- + H_2O$

537 Metastable hydromagnesite is well documented in heavily weathered ultramafic
538 rocks (Mumpton et al. 1965; Mumpton & Thompson 1966; Brideau et al. 2007) when
539 CO_2-bearing groundwater is available at shallow depth. Hydromagnesite probably
540 precipitated directly from magnesium and bicarbonate-rich solutions at
541 temperatures around 25-30 ˚C based on the $\delta^{18}O$ values.

542 The near-surface water chemistry data in our study has some typical characteristics
543 of spring waters from weathered ultramafic rocks (Barnes & O'Neil 1969, O'Neil &
544 Barnes 1971, Papastamataki 1977), but with important differences. On the whole,
545 published ultramafic spring water data have higher pH (9.95-11.86) than in our
546 study, and lower Mg/Ca ratios typically <0.1 and only rarely up to ~8 (e.g. Cipolli et
547 al. 2004, Marques et al. 2008). Spring waters from Mesozoic peridotites and
548 serpentinites, that host vein and stockwork magnesite deposits (but not
549 hydromagnesite or huntites), have pH values 7.5-9.3, lower magnesium contents
550 (max 127 ppm), higher calcium contents (9 ppm - 66 ppm) and low molar Mg/Ca
551 ratio (mean <4) (Stamatis & Gartzos 1999).

552 Spring waters near Schinos, where hydromagnesite cotton-balls are particularly
553 widespread, have the highest pH values in our study (9 to 9.3), Mg^{2+} of 87 to 89 mg
554 L^{-1} and a high molar Mg/Ca ratio ~180 (Table 3). These characteristics are
555 consistent with water in equilibrium with atmospheric CO_2 (modelled in REACT;
556 Bethke 1996) and supersaturated with respect to magnesite, but with the high

Mg/Ca ratio providing impetus for hydromagnesite rather than magnesite precipitation (Müller et al. 1972). The low Ca^{2+} concentrations largely prevented aragonite formation, excepting a few local occurrences. The isotopic values of the hydromagnesites, despite possible disequilibrium effects, are mostly consistent with a shallow meteoric-sourced fluid around 25-30 ˚C with CO_2 sourced mainly from the atmospheric and/or soil CO_2 in the surface weathering zone.

The minor but significant presence of pyroaurite group minerals is best explained by partial oxidation of soluble Fe^{2+}, liberated from mineral decomposition (Hansen & Taylor 1990; Taylor et al. 1991). We note that a pCO_2 below 10^{-6} atm. allows brucite conversion to pyroaurite group minerals (Hostetler 1960; Hostetler et al. 1966), although as at New Idria (Mupton & Thompson 1966), brucite is typically not preserved (now dissolved?) in the heavily weathered zones.

In the Schinos area (LS-1, Fig. 1), the Mg-HCO_3 waters also have high Cr(VI) concentrations (up to 120 µg/L; Pyrgaki et al. 2016). This water chemistry promotes formation of a Mg-Fe-(Ni-rich) hydroxyl-carbonate type mineral of the pyroaurite group ($Mg_6Fe^{3+}_2(CO_3)(OH)_{16}•4H_2O$). This is similar to the Querceto area of coastal Tuscany (Langone et al. 2013) where spring waters, sourced from serpentinite bedrock with Fe-rich brucite, show evidence for ongoing brucite dissolution coupled with precipitation of hydromagnesite as crusts and veinlets, accompanied by minor Mg-rich layered double hydroxides. These Ni^{2+} and Cr^{3+} rich layered double hydroxide group minerals behave as an electrochemical cell promoting the oxidative leaching of Cr^{3+} as the soluble CrO_4^{2-} ion. Pyroaurite group mineralization in the present study was probably restricted to a shallow groundwater mixing zone, just below the groundwater table where Eh-pH characteristics allowed their formation (Taylor et al. 1991).

In this study huntite was only found close to the Soussaki volcanic centre where the groundwater molar Mg/Ca ratio is ~3.5 (Kelepertsis et al. 2001). This value is low compared with the high Mg/Ca ratios measured in the north study area spring waters where hydromagnesite is common, and suggests that huntite formed as diagenetic transformation of early formed hydromagnesite by locally sourced Ca-rich fluids (see also Alderman 1965; Kinsman 1967; Stamatakis 1995). The $\delta^{18}O$ values imply fluid temperatures ~30 ˚C during diagenetic transformation and the

589 huntite $\delta^{13}C$ values, mostly between -4 and +2‰, are consistent with some CO_2
590 and Ca^{2+} sourced from decarbonation/dissolution of basement limestone. Most of
591 the non-vein magnesites have similar isotopic compositions to the huntites and
592 may originate by dehydration reactions (see Mumpton & Thompson 1966;
593 Hostetler et al. 1966; Zhang et al. 2000).

594 In the north of the study area, dehydration of hydromagnesite to magnesite (Zhang
595 et al. 2000; Hänchen et al. 2008; Boschi et al. 2009) may explain the presence of
596 'lettuce leaf' magnesite with colloform texture stratigraphically above
597 hydromagnesite at near-surface outcrops: at least 3 magnesite samples (blue dots
598 Fig. 9) have disequilibrium isotopic characteristics (particularly the very negative
599 $\delta^{13}C$ values) consistent with meteoric-sourced fluids around 25 ˚C with CO_2 mainly
600 from the atmosphere.

601 The five vein-type magnesites may represent an earlier phase of mineralization
602 associated with more active volcanic conditions, regional extensional stress and
603 abundant geothermal CO_2. Three of the isotopic compositions are consistent with
604 those described by Fallick et al. (1991) for Yugoslavian magnesite deposits. This
605 said, we cannot be confident that their compositions have not re-equilibrated with
606 cooler hydrothermal and weathering fluids.

607

608 ## Conclusions

609

610 In common with other studies of Mg-(hydro)carbonate mineralization in
611 serpentinized ultramafic rock masses, the serpentinizing fluids and subsequent
612 infiltrating groundwaters exploited structural conduits, both thrust-associated and
613 from normal faulting. The latter faulting initiated in the late Pliocene (Gawthorpe et
614 al. 2017) and continues to the present day. These normal faults may provide the
615 main connection between the shallow subsurface and deeper zones deformed by
616 Alpine tectonics. Thus mineralization is broadly syn-tectonic, but it post-dates Alpine
617 compression. Structural routing of fluids helped control the position of the local
618 water table to enable near-surface weathering and carbonation within the rock
619 mass. Further, in common with a number of recent studies, our Mg-

(hydro)carbonate $\delta^{18}O$ values suggest that most of the Mg-(hydro)carbonate mineralization occurred at temperatures between 25-30 ˚C despite the proximity of a volcanic centre with fluid temperatures locally up to 70 ˚C.

Our study shows specifically that:

1. Despite the proximity of a volcanic centre with strong CO_2 flux, 75% of the carbon isotope data imply little or no incorporation of this CO_2 into the authigenic Mg-(hydro)carbonate. Indeed, $\delta^{13}C$ more negative than -6‰, may be influenced by disequilibrium effects associated with high pH fluids. In our study, local area calcrete $\delta^{13}C$ fixes the most likely negative equilibrium calcite value to ~-10‰. If the predicted fractionation offset between calcite and magnesite (Deines 2008) is robust, then equilibrium magnesite values from groundwater equilibrated with soil CO_2 at 20 ˚C are unlikely to be below -6‰. The importance of this effect may have been overlooked in earlier studies.
2. In common with most work on low temperature magnesite mineralization, precise $\delta^{18}O$-derived temperatures are not resolvable, partly because the parent fluid composition is not well-enough constrained, partly because the extent of fluid mixing is unknown, and also because the magnesite-water fractionation factor is not fully resolved (Chako & Deines 2008). This also makes potential disequilibrium effects on Mg-(hydro)carbonate $\delta^{18}O$ difficult to assign. These issues may simplify as the temperature dependence of clumped isotopes in magnesites are explored further, following the lead of Quesnel et al. (2016) and García del Real et al. (2017).
3. At the outcrop scale we have some evidence to suggest that hydromagnesite will dehydrate under near-surface conditions to cauliflower or botryoidal-nodular magnesites. Local formation of huntite, at shallow depths, is attributed to the diagenetic transformation of the earlier-formed hydromagnesite by Ca-rich fluids located near to the volcanic centre.

Acknowledgements

Analytical work was done at the National and Kapodistrian University of Athens (NKUA) Department of Geology and Geoenvironment, excepting stable isotope analyses which were made at the Scottish Universities Environmental Research Centre (SUERC) in East Kilbride, Scotland. We are very grateful to Dr Manolis Skourtsos (NKUA) who helped prepare Figure 1. Alex Brasier (Aberdeen) kindly allowed us to use some of his unpublished calcrete data.

References

Aharon, P. 1988. A stable-isotope study of magnesites from the Rum Jungle Uranium Field, Australia: implications for the origin of strata-bound massive magnesites. *Chemical Geology*, **69**, 127–145.

Alderman, A.R. 1965. Dolomite sediments and their environment in the south-east of South Australia. *Geochimica et Cosmochimica Acta*, **29**, 1355-1365.

Anonymous. 1999. Low Enthalpy Geothermal Energy Driven Sea Water Desalination Plant at Sousaki Korinthos. Center for Renewable Energy Sources, Project **GE/00339/95**, Athens, Greece.

Andrews, J.E., Gare, S.G. & Dennis, P.F. 1997. Unusual isotopic phenomena in Welsh quarry water and carbonate crusts. *Terra Nova*, **9**, 67-70.

Barnes, I. & O'Neil, J.R. 1969. The relationship between fluids in some fresh Alpine-type ultramafics and possible modern serpentinization, Western U.S. *Geological Society of America Bulletin*, **80**, 1947-1960.

Barnes, I., LaMarche,V.C. & Himmelberg, G. 1967. Geochemical evidence of present -day serpentinization. *Science*, **156**, 830-832.

Bentham, P., Collier, R.E.Ll., Gawthorpe, R. L., Leeder, M.R., Prossor, S. & Stark, C. 1991. Tectono-sedimentary development of an extensional basin: the Neogene Megara Basin, Greece. *Journal of the Geological Society London*, **148**, 923-934.

681 Bethke, C. 1996. *Geochemical Reaction Modelling: Concepts and Applications*,
682 New York, Oxford University Press, 397pp.

683 Bornovas, J., et al. 1984. Geological map of Greece 1:50.000, Sheet Kaparelli
684 Geological map of Greece 1:50.000, Sheet Sofiko IGME publications, Athens.

685 Boschi. C., Dini, A., Dallai, L., Ruggieri, G. & Gianelli, G. 2009. Enhanced CO_2-
686 mineral sequestration by cyclic hydraulic fracturing and Si-rich fluid infiltration
687 into serpentinites at Malentrata (Tuscany, Italy). *Chemical Geology*, **265**, 209-
688 226.

689 Bowen, G.J. & Revenaugh, J. 2003. Interpolating the isotopic composition of
690 modern meteoric precipitation. *Water Resources Research*, **39**, 1299-1312.

691 Brasier, A.T. 2007. *Palaeoenvironmental Reconstructions from Quaternary Tufas*
692 *and Calcretes, Central Greece*. PhD thesis, University of East Anglia, 293 pp.

693 Brideau, M.A., Stead, D., Roots, C. & Orwin, J. 2007. Geomorphology and
694 engineering geology of a landslide in ultramafic rocks, Dawson City, Yukon.
695 *Engineering Geology*, **89**, 171-194.

696 Brydie, J.R., Fallick, A.E., Ilich, M., Maliotis, G. & Russell, M.J. 1993. A stable
697 isotopic study of magnesite deposits in the Akamas area, N.W. Cyprus:
698 *Institution of Mining and Metallurgy Transactions*-B, **102**, B50–B53.

699 Cassard, D. 1980. *Structure et origine des gisements de chromite du Massif du Sud*
700 *(ophiolite de Nouvelle Calédonie)*. *Guides de prospection*. Thèse Doc. 3˚ Cycle,
701 Univ. Nantes, 152pp.

702 Chako, T. & Deines, P. 2008. Theoretical calculation of oxygen isotope fractionation
703 factors in carbonate systems. *Geochimica et Cosmochimica Acta*, **72**, 3640-
704 3660.

705 Chidester, A.H., Albee, A.L. & Cady, W.M. 1978. Petrology, structure and genesis
706 of the asbestos bearing ultramafic rocks of the Belvider mountain area in
707 Vermont. US Geological Survey Professional paper **1016**.

708 Cipolli, F., Gambardella, B., Marini, L., Ottonello, M & Zuccolini, V. 2004.
709 Geochemistry of high-pH waters from serpentinites of the Gruppo di Voltri

(Genova, Italy) and reaction path modelling of CO_2 sequestration in serpentinite aquifers. *Applied Geochemistry*, **19**, 787-802.

Clark, I.D., Fontes, J-C. & Fritz, P. 1992. Stable isotope disequilibria in travertine from high pH waters: laboratory investigations and field observations from Oman. *Geochimica et Cosmochimica Acta*, **56**, 2041-2050.

Collie,r R.E.Ll. & Dart, C.J. 1991. Neogene to Quaternary rifting, sedimentation and uplift in the Corinth Basin, Greece. *Journal of the Geological Society of London*, **148**, 1049-1065.

Craig, H. 1961. Isotopic variations in meteoric waters. *Science*, **133**, 1833-1834.

D'Alessandro, W., Kyriakopoulos, K., Rotolo, S., Bagnato, M., Bruno, C., Casa, G., Minio, M. & Plicanti, F. 2005 Natural degassing activity of the geothermal system of Sousaki (Greece): Environmental impact and gas hazard issues. ICGG8, 8th International Conference Gas Geochemistry, Oct. 2-8, Palermo and Milazzo, Italy, 2005.

D'Alessandro, W., Brusca, L., Kyriakopoulos, K., Rotolo, S., Michas, G., Minio, M. & Papadakis, G. 2006. Diffuse and focused carbon dioxide and methane emissions from the Sousaki geothermal system, Greece. *Geophysical Research Letters*, **33**, pp 5, L05307, doi 10.1029/2006GL025777.

Das Sharma, S., Patil, D.J. & Gopalan, K. 2002. Temperature dependence of oxygen isotope fractionation of CO_2 from magnesite-phosphoric acid. *Geochimica et Cosmochimica Acta*, **66**, 589-593.

Deines, P. 2008. Carbon isotope effects in carbonate systems. *Geochimica et Cosmochimica Acta*, **68**, 2659-2679.

Demange, J. & Gauthier, B. 1992. Soussaki Geothermal Project, Greece. Unpublished Report. **92CFG57**, GEMEE, Athens.

De Wit, M., Dutch, S., Kligfield, R., Allen, R. & Stern, C. 1977. Deformation, serpentinization and emplacement of a dunite complex, Gibbs Island, South Shetland Islands: possible fracture zone tectonics. *Journal of Geology*, **85**, 745-762.

739 Donnelly, T., Waldron, S., Tait, A., Dougans, J. & Bearhop, S. 2001. Hydrogen
740 isotope analysis of natural abundance and deuterium-enriched waters by
741 reduction over chromium on-line to a dynamic dual inlet isotope-ratio mass
742 spectrometer. *Rapid Communications in Mass Spectrometry*, **15**, 1297-1303.

743 Dotsika, E., Poutoukis, D., Michelot, J.L. & Raco, B. 2009. Natural tracers for
744 identifying the origin of the thermal fluids emerging along the Aegean Volcanic
745 arc (Greece): Evidence of Arc-Type Magmatic Water (ATMW) participation.
746 *Journal of Volcanology and Geothermal Research*, **179**, 19-32.

747 Dotsika, E., Lykoudis, S. & Poutoukis, D. 2010. Spatial distribution of isotopic
748 composition of precipitation and spring water in Greece. *Global and Planetary*
749 *Change*, **71**, 141-149.

750 Epstein, S. & Mayeda, T. 1953. Variation of O^{18} content of waters from natural
751 sources. *Geochimica et Cosmochimica Acta*, **4**, 213-224.

752 Eslami, A., Stamatakis, M.G., Perraki, M., Vasilatos, C. & Hollingberry, L. 2015. On
753 the occurrence of Mg- and Fe-rich carbonate mineral assemblages hosted in the
754 Nain ophiolite melange, central Iran and their industrial potential. *Neus Jahrbuch*
755 *für Mineralogie – Abhandlungen*, **192**, 59-71.

756 Fallick, A.E., Ilich, M. & Russell, M.J. 1991. A stable isotope study of the magnesite
757 deposits associated with the Alpine-type ultramafic rocks of Yugoslavia.
758 *Economic Geology*, **86**, 847–861.

759 Fourcade, S., Trotington, L., Boulvais, P., Techer, M.E., Vandamme, D., Salameh,
760 E. & Khoury, H. 2007. Cementation of kerogen-rich marls by alkaline fluids
761 released during weathering of thermally metamorphosed marly sediments. Part
762 I: Isotopic (C, O) study of the Khushaym Matruk natural analogue (central
763 Jordan). *Applied Geochemistry*, **22**, 1293-1310.

764 Fytikas, M., Innocenti, F., Kolios. N., Manetti, P. & Mazzuoli, R. 1986. The Plio-
765 Quaternary Volcanism of Saronikos area (Western part of the Active Aegean
766 Volcanic Arc). *Annales Géologiques Des Pays Helléniques*, **33**, 23-45.

767 Gaitanakis, P., Mettos, A. & Fytikas, M. 1985. Geological map of Greece 1:50.000,
768 Sheet Sofikon Geological map of Greece 1:50.000, Sheet Sofikon IGME
769 publications, Athens.

770 García del Real, P., Maher, K., Kluge, T., Bird, D.K., Brown Jr., G.E., & John, C.M.
771 2016. Clumped-isotope thermometry of magnesium carbonates in ultramafic
772 rocks. *Geochimica et Cosmochimica Acta*, **193**, 222-250.

773 Gartzos, E. 2004. Comparative stable isotopes study of the magnesite deposits of
774 Greece. *Bulletin of the Geological Society of Greece*, **34**, 196-203.

775 Gawthorpe, R.L., Leeder, M.R., Kranis, H., Skourtsos, E., Andrews, J.E., Henstra,
776 G.A., Mack, G.H., Muravchik, M., Turner, J.A. & Stamatakis 2017. Tectono-
777 sedimentary evolution of the Plio-Pleistocene Corinth rift, Greece. *Basin*
778 *Research*, 1-32, doi: 10.1111/bre.12260

779 Hänchen, M., Prigiobbe, V., Baciocchi, R. & Mazzotti, M. 2008. Precipitation in the
780 Mg-carbonate system - effects of temperature and CO_2 pressure. *Chemical*
781 *Engineering Science*, **63**, 1012-1028.

782 Hansen, H.C.B. & Taylor, R.M. 1990. Formation of synthetic analogues of double
783 metal-hydroxy carbonate minerals under controlled pH conditions: I. The
784 synthesis of pyroaurite and reevesite. *Clay Minerals*, **25**, 161-179.

785 Hostetler, P.B. 1960. *Low temperature relations in the system: MgO-SiO_2-CO_2 H_2O*.
786 Ph.D. thesis, Harvard University, Cambridge, Mass. 168pp.

787 Hostetler, P.B., Coleman, R.G., Mumpton, F.A. & Evans, B.W. 1966. Brucite in
788 Alpine serpentinites. *American Mineralogist*, **51**, 75-98.

789 Jedrysek, M.O. & Halas, S. 1990. The origin of magnesite deposits from the Polish
790 Foresudetic Block ophiolites: Preliminary $\delta^{13}C$ and $\delta^{18}O$ investigations. *Terra*
791 *Nova*, **2**, 154–159.

792 Kadir, S., Kolayli, H. & Eren, M. 2013. Genesis of sedimentary- and vein-type
793 magnesite deposits at Kop Mountain, NE Turkey. *Turkish Journal of Earth*
794 *Sciences*, **22**, 98-114.

795 Kaplanis, A., Koukouvelas, I., Xypolias, S. & Kokkalas, S. 2013. Kinematics and
796 ophiolite obduction in the Gerania and Helicon Mountains, central Greece.
797 *Tectonophysics*, **595–596**, 215–234.

798 Kahya, A. & Kuşcu, M. 2014. Source of the mineralizing fluids in ultramafic related
799 magnesite in the Eskişehir area, northwest Turkey, along the Izmir–Ankara
800 Suture: a stable isotope study. *Turkish Journal of Earth Sciences*, **23**, 1-15.

801 Kelemen, P. & Matter, J. 2008. *In situ* carbonation of peridotite for CO_2 storage.
802 *Proceedings of the National Academy of Science*, **105**, 17295-17300.

803 Kelemen, P., Matter, J., Streit, E., Rudge, J., Curry, W. & Bluszatajn, J. 2011. Rates
804 and mechanisms of mineral carbonation in peridotite: natural processes and
805 recipies for enhanced, *in situ* CO_2 capture and storage. *Annual Review of Earth*
806 *and Planetary Sciences*, **39**, 545-576.

807 Kelepertsis, A., Alexakis, D. & Kita, I. 2001. Environmental geochemistry of soils
808 and waters of Sousaki area, Korinthos, Greece. *Environmental Geochemistry*
809 *and Health*, **23**, 117-135.

810 Kinsman, D. 1967. Huntite from a carbonate evaporate environment. *American*
811 *Mineralogist*, **52**, 1332-1340.

812 Kyriakopoulos, K.G., Kanaris-Sotiriou, R. & Stamatakis, M.G. 1990. The authigenic
813 minerals formed from volcanic emanations at Soussaki, west Attica peninsula,
814 Greece. *Canadian Mineralogist*, **28**, 363-368.

815 Langone, A., Baneschi, I. Boschi, C., Dini, A., Guidi, M. & Cavallo, A. 2013.
816 Serpentinite-water interaction and chromium(VI) release in spring waters:
817 example from Tuscan ophiolites. *Ofioliti*, **38**, 41-57.

818 Leeder, M.R., Portman, C., Andrews, J.E., Collier, R.E.Ll., Finch, E., Gawthorpe,
819 R.L., McNeill, R.C., Pérez-Arlucea, M. & Rowe, P. 2005. Normal faulting and
820 crustal deformation, Alkyonoides Gulf and Perachora Peninsula, eastern Gulf of
821 Corinth Rift, Greece. *Journal of the Geological Society of* London, **162**, 549-561.

822 Leeder, M.R., Mack, G.H., Brasier, A.T., Parrish, R.R., McIntosh, W.C., Andrews,
823 J.E. & Duermeijer, C. 2008. Late-Pliocene timing of Corinth (Greece) rift-margin
824 fault migration. *Earth and Planetary Science Letters*, **274**, 132-141.

825 Marques, J.M., Carreira, P.M., Carvalho, M.R., Matias, M.J, Goff, F.E., Basto, M.J.,
826 Graça, R.C., Aires-Barros, L. & Rocha, L. 2008. Origins of high pH mineral
827 waters from ultramafic rocks, Central Portugal. *Applied Geochemistry*, **23**, 3278-
828 3289.

829 Marinos, G. 1951. The lignite basin of Megara. Institute of Geological and Mineral
830 Exploration, Geological Reconnaissance No. 3, Athens, IGME Publications, 22
831 pp.

832 McCrea, J.M. 1950. On the isotopic chemistry of carbonates and a paleotemperature
833 scale. *Journal of Chemical Physics*, **18**, 849-857.

834 Mettos, A., Gaitanakis, P., Rontogianni, Th., Bavay, Ph., Loakim, Chr., Mitsaki, V. &
835 Koutsouveli, A. 1982. Geological Study of "Loutraki-Sousaki" Region.
836 Geothermal Researches, IGME, Greece, 65 pp.

837 Mettos, A., Rontogianni, Th. & Bavay, Ph. 1988. Plio-Pleistocene deposits of the
838 Soussaki-Ag. Theodori area (Corinth): Stratigraphy-deformation. *Bulletin of the*
839 *Geological Society of Greece*, **20**, 91-111.

840 Möller, P. 1989. Nucleation processes of magnesite. *In*: Möller, P. (ed.) *Magnesite:*
841 *Geology, Mineralogy, Geochemistry and Formation of Mg-carbonates*.
842 Monograph Series on Mineral Deposits 28, pp. 287-292. Gebrüder Borntraeger
843 Verlagsbuchhandlung, Science Publication, Stuttgart.

844 Müller, G., Irion, G. & Förstner, U. 1972. Formation and diagenesis of inorganic Ca-
845 Mg carbonates in the lacustrine environment. *Naturwissenschaften*, **59**, 158-
846 164.

847 Mumpton, F.A. & Thompson, C.S. 1966. The stability of brucite in the weathering
848 zone of the New Idria serpentinite. *Clays and Clay Minerals*, Proceedings of
849 National Conference No. **I4** (1965), 249-257.

850 Mumpton, F.A., Jaffe, H.W. &Thompson, C.S. 1965. Coalingite, a new mineral from
851 the New Idria Serpentinite, Fresno and San Benito Counties, California.
852 *American Mineralogist*, **50**, 1893-1913.

853 Norrell, G.T., Teixell, A. & Harper ,G.D. 1989. Microstructure of serpentinite
854 mylonites from the Josephine ophiolite and serpentinization in retrogressive
855 shear zones. *Geological Society of America Bulletin*, **101**, 673-682.

856 O'Neil, J.R. & Barnes, I. 1971. ^{13}C and ^{18}O compositions in some fresh-water
857 carbonates associated with ultramafic rocks and serpentinites: Western United
858 States. *Geochimica et Cosmochimica Acta*, **35**, 687–697.

859 Okamoto, I., Mizuochi, Y., Ninomiya, A., Kato, T., Yajima, T. & Ohsumi, T. 2006. In-
860 situ test on CO_2 fixation by serpentinite rock mass in japan. 8th International
861 Conference on Greenhouse Gas Control Technologies (GHGT-8), Trondheim,
862 Norway, 19-22 June 2006. Volume 1, pp. 475-480. Elsevier Science Ltd, ISBN
863 978-1-60560-353-7.

864 Oskierski, H.C., Bailey, J.G., Kennedy, E.M., Jacobsen, G., Ashley, P.M. &
865 Dlugogoski, B.Z. 2013. Formation of weathering-derived magnesite deposits in
866 the New England Orogen, New South Wales, Australia: implications from
867 mineralogy, geochemistry and genesis of the Attunga magnesite deposit.
868 *Mineralium Deposita*, **48**, 525–541.

869 Panichi, C., La Ruffa, G., Kavouridis, T., Leontiadis, G., Leonis, C., Liberopoulou,
870 V. & Dotsika. E. 2000. Geochemical Assessment of the Thermal Fluids Emerging
871 along the Aegean Volcanic Arc (Greece). Proceed. World Geothermal Congress,
872 Kyushu-Tohoku, Japan, May 28 - June 10, 2000.

873 Papastamataki, A. 1977. The alkalinity and the chemical composition of springs
874 issuing from peridotites. *Annales Géologiques Des Pays Helléniques*, **27**, 551-
875 566.

876 Papp, A. & Steininger, F.F. 1979. The Pliocene of the Megara Graben. Examples of
877 marine/brackish limnic cycles triggering the evolution of endemic mollusc faunas.
878 Field Guide to the Neogene of Megara-Peloponnisos-Zakynthos. Publications of
879 the NKUA, Deptartment of Geology & Paleontology, Series A, No 34, pp. 3-16.

880 Park, A. & Fan, L. 2004. CO_2 mineral sequestration: physically activated dissolution
881 of serpentine and pH swing process. *Chemical Engineering Science*, **59**, 5241-
882 5247.

883 Pe-Piper, G. & Hatzipanagiotou, K. 1997. The Pliocene volcanic rocks of
884 Crommyonia, western Greece and their implications for the early evolution of the
885 South Aegean Arc. *Geological Magazine*, **134**, 55-66.

886 Pyrgaki, K., Argyraki, A., Kelepertzis, E., Paraskevopoulou, V., Botsou, F.,
887 Dassenakis, E., Mitsis, I. & Skourtsos, E. 2016. Occurrence of hexavalent
888 chromium in the ophiolite related aquifers of Loutraki and Schinos areas. Bulletin
889 of the Geological Society of Greece, 50, Proceedings of the 14th International
890 Congress, Thessaloniki, 10 pp.

891 Quesnel, B., Gautier, P., Boulvais, P., Cathelineau, M., Maurizot, P., Cluzel, D.,
892 Ulrich, M., Guillot, S., Lesimpl,e S. & Couteau, C. 2013. Syn-tectonic, meteoric
893 water-derived carbonation of the New Caledonia peridotite nappe. *Geology*, **41**,
894 1063–1066.

895 Quesnel, B., Boulvais, P., Gautier, P., Cathelineau, M', John, C., Dierick, M.,
896 Agrinier, P. & Drouillet, M. 2016. Paired stable isotopes (O, C) and clumped
897 isotope thermometry of magnesite and silica veins in the New Caledonia
898 Peridotite Nappe. *Geochimica et Cosmochimica Acta*, **183**, 234-249.

899 Rosenbaum, J. & Sheppard, S.M.F. 1986. An isotopic study of siderites, dolomites
900 and ankerites at high temperatures. *Geochimica et Cosmochimica Acta*, **50**,
901 1147-1150.

902 Sayles, F.L. & Fyfe, W.S. 1973. Crystallization of magnesite from aqueous-solution.
903 *Geochimica et Cosmochimica Acta*, **37**, 87–99.

904 Schroll, E. 2002. Genesis of magnesite deposits in the view of isotope geochemistry.
905 *Boletim Paranaense de Geociencias*, **50**, 59-68, Editora UFPR, IGCP 443.

906 Smoot, J.P. & Lowenstein, T.K. 1991. Chapter 3: Depositional environments of
907 non-marine evaporites. *In*: Melvin, J.L. (ed.) *Evaporites, Petroleum and*
908 *Mineral Resources*. Developments in Sedimentology **50**, Elsevier, Amsterdam,
909 189-347.

910 Spiliadis, Th. 1965. Olonos-Pindos Schichten in der Perachora-Halbinsel und
911 geologische Vereingung des Attica-Megaris-Geraneia Gebietes. *Bulletin of the*
912 *Geological Society of Greece*, **6**, 196-214.

913 Stamatakis, M.G. 1995. Occurrences and genesis of huntite-hydromagnesite
914 assemblages, Kozani, Greece-important new white fillers and extenders.
915 *Institution of Mining and Metallurgy Transactions*-B, **104**, 179-186.

916 Stamatakis, M.G. & Mitsis, I. 2013. The occurrences of Mg-hydroxycarbonates in
917 serpentinites of the western section of the South Aegean Volcanic Arc (west
918 Attica peninsula-northeastern Argolis peninsula), Greece. *Bulletin of the*
919 *Geological Society of Greece*, **47**, Proceedings of the 13th International
920 Congress, Chania, Sept. 2013, 13 pp

921 Stamatis, G., & Gartzos, E. 1999. The silica supersaturated waters of northern Evia
922 and eastern central Greece. *Hydrological Processes*, **13**, 2833-2845.

923 Stanger. G. & Neal, C. 1994. The occurrence and chemistry of huntite from Oman.
924 *Chemical Geology*, **112**, 247-254.

925 Stevula, L., Petrovic, J. & Kubranova, M. 1978. Formation of synthetic magnesite by
926 carbonatization of hydromagnesite under hydrothermal conditions. *Chemické*
927 *Zvesti*, **32**, 441–443.

928 Stiros, S. 1995. The 1953 seismic surface fault: implications for the modelling of the
929 Sousaki (Corinth area, Greece) geothermal field. *Journal of Geodynamics*, **20**,
930 167-180.

931 Stumm, W. 1992. *Chemistry of the Solid–Water Interface*. Wiley-Interscience, New
932 York, pp. 523–598.

933 Tarutani, T., Clayton, R. N. & Mayeda, T. K. 1969. The effect of polymorphism and
934 magnesium substitution on oxygen isotope fractionation between calcium
935 carbonate and water. *Geochimica et Cosmochimica Acta*, **33**, 987–996.

936 Taylor, R.M., Hansen, H.C.B., Stanger, G. & Bender Koch, C. 1991. On the genesis
937 and composition of natural pyroaurite. *Clay Minerals*, **26**, 297-309.

938 Teir, S., Eloneva, S., Fogelholm, C.J. & Zevenhoven, R. 2009. Fixation of carbon
939 dioxide by producing hydromagnesite from serpentinite. *Applied Energy*, **86**,
940 214-218.

941 Usdowski, E. & Hoefs, J. 1986. $^{13}C/^{12}C$ partitioning and kinetics of CO_2 absorption
942 by hydroxide buffer solutions. *Earth and Planetary Science Letters*, **80**, 130–134.

943 Usdowski, E. & Hoefs, J. 1988. $^{13}C/^{12}C$ fractionation during the chemical absorption
944 of CO_2 gas by the NH_3-NH_4Cl buffer. *Chemical Geology (Isotope Geoscience*
945 *Section)*, **73**, 79-85.

946 Usdowski, E. & Hoefs, J. 1990. Kinetic $^{13}C/^{12}C$ and $^{18}O/^{16}O$ effects upon dissolution
947 and outgassing of CO_2 in the system CO_2-H_2O. Chemical Geology (Isotope
948 Geoscience Section), 80, 109-118.

949 Vakondios, L. 1996. *Study of the chromite metallogenesis associated with*
950 *Mediterranean type ophiolites. An example from Tinos Island and Gerania Mt.,*
951 *Attica, Greece.* Ph.D Thesis, University of Patras, Patras, 120pp.

952 Vrellis, G., Kavouridis, Th. & Dovelos, J. 1991. Geothermal Study of the Sousaki
953 area. Report IGME, Athens, 71 pp

954 Wilson, S., Dipple, G., Power, I., Thom, J., Anderson, R., Raudsepp, M., Gabites, J.
955 & Southam, G. 2009. Carbon dioxide fixation within mine wastes of ultramafic-
956 hosted ore deposits: examples from the Clinton Creek and Cassiar chrysotile
957 deposits, Canada. *Economic Geology*, **104**, 95–112.

958 Zedef, V., Russell, M.J., Fallick, A.E. & Hall, A.J. 2000. Genesis of vein stockwork
959 and sedimentary magnesite and hydromagnesite deposits in the ultramafic
960 terranes of southwestern Turkey: a stable isotope study. *Economic Geology*, **95**,
961 429-446.

962 Zhang, P.C., Anderson, H.L., Kelly, J.W., Krumhansl, J.L. & Papenguth, H.W.
963 2000. Kinetics and Mechanisms of Formation of Magnesite from
964 Hydromagnesite in Brine. US-Gov. Report- OSTI DE00764025.

965

966 **Figure and Table Captions**

967 **Fig. 1.** (a) Locality and geological map of the study area, with inset map showing
968 the study area in Greece. Lithologies: 1 Modern alluvium and scree; 2 Plio–
969 Pleistocene sediments 3 Plio-Pleistocene volcanics; 4 Middle–Upper Jurassic
970 serpentinites; 5 Upper Jurassic–Lower Cretaceous clastic sediments; 6 Middle
971 Jurassic–Lower Cretaceous Limestones; 7 Pleistocene-Recent faults and thrusts
972 (and inferred faults and thrusts). The star symbol marks the position of the Soussaki

973 Volcanic centre. LS-X shows the position of mineralogical and water samples taken
974 in this study, details of which are given in Tables 1-4. The Holocene-active
975 Schinos/Pisia fault strand is located just south of Schinos and goes offshore near
976 LS-1. (b) Schematic geological section through upper part of the nappe pile in NE
977 of the study area (LS-2 on Fig. 1a) showing Jurassic serpentinites overthrust by
978 Cretaceous limestones. Intense alteration of the serpentinites and hydromagnesite
979 mineralization occurs in a zone immediately below the thrust contact. Below this
980 altered zone the serpentinite is relatively unaltered.

981 **Fig. 2.** (a) Type 1 white mineral assemblages of magnesite (MG), huntite (H) and
982 hydromagnesite (HYM) as stringers, veinlets and cotton ball nodules in highly
983 altered earthy serpentinite close to the Soussaki volcanic centre (LS-8 Fig. 1; s-
984 107 samples, Table 1). Hammer is 30 cm long. (b) Type 2 vein magnesite cross-
985 cutting Neogene marls that overlie the Mesozoic ultramafics. S study area near
986 Ag. Dimitrios, LS-7 on Fig. 1. Hammer is 30 cm long.

987 **Fig. 3.** Representative x-ray diffraction patterns and SEM images. (a) magnesite:
988 SEM inset shows rhombohedral, closely-packed, euhedral magnesite crystals that
989 make up magnesite nodules (samples from LS6 and 8 in Fig. 1). (b)
990 hydromagnesite: left SEM inset shows tabular, euhedral hydromagnesite crystals
991 developed in pores spaces; smaller early formed hydromagnesite forms the pore
992 rim; right SEM inset shows detail (white box in left image) of pore-filling tabular
993 hydromagnesite (samples from LS-1 and 2 in Fig. 1). (c) huntite: SEM inset shows
994 euhedral rhombohedral huntite that forming a closely packed earthy mass (samples
995 from LS6 in Fig. 1).

996 **Fig. 4.** Type 1 (hydro)magnesites. (a) Botryoidal (cauliflower heads) of snow-white
997 magnesite hosted in earthy altered serpentine. (b) Cauliflower head magnesite
998 nodules in highly altered-earthy serpentinite. S study area near Ag Theodoroi (Fig.
999 1; Ag. Theod. samples, Table 1). Camera case is 12 cm long. (c) Hydromagnesite
1000 cotton balls in highly altered bedrock above a prominent fault plane (white dashed
1001 line). There are no hydromagnesite cotton balls in bedrock below (left of) the fault.
1002 The fault may delineate the margin of a diatreme-like occurrence of alteration. (d)
1003 Detail of 3(c) showing hydromagnesite cotton balls in highly altered bedrock.

Camera case is 8 cm wide. S study area near Ag Marina (LS-6, Fig. 1; sample AG-TH-4-11, Table 1).

Fig. 5. Type 1 (hydro)magnesites. (a) Network of magnesite veins in indurated and tectonized serpentinite bedrock. S central study area near Metalleio. (LS-5, Fig. 1; sample 10, Table 1). Outcrop is about 2 m high. (b) Crystalline botryoidal radiating hydromagnesite efflorescence on fracture surfaces in serpentinite. Central study area (LS-3, Fig. 1; sample f2b, Table 1). 2 Euro coin is 2.6 cm diameter.

Fig. 6. Field morphology of Type 1 Mg-(hydro)magnesites in N study area near Alepochori (LS-2, Fig. 1). (a) Cotton ball assemblages and veinlets of hydromagnesite developed as 'honeycomb' within altered/earthy serpentine. Note hydromagnesite rimming rounded blocks of more resistant partially altered serpentine. (Sample ALEPO-2, Table 1). Hammer is 30 cm long. (b) Highly brecciated earthy serpentinite, strongly mineralized by hydromagnesite. Outcrop is about 6 m high. (c) Hard asymmetric crusts of magnesite around bedrock cores (near the pen) and nodules, cotton-balls and fissure fillings of hydromagnesite in altered serpentinite. (Sample AL2CF, Table 1). Pen is 15 cm long. (d) Fissures and groundmass filled with white earthy hydromagnesite and nodular hydromagnesite, developed in earthy serpentine in the vicinity of shear zones. These vein-fills occur in the weathered rock and in cracks through more indurated host rock that was more resistant to weathering. Pocket knife is 16 cm long.

Fig. 7. (a) Altered/earthy serpentine with Type 1 cotton ball assemblages of hydromagnesite, N study area near Alepochori (LS-2, Fig. 1). Veinlets of hard magnesite have developed in a discrete zone above level of notebook. These veinlets have 'lettuce leaf' morphology when seen weathering out in three dimensions. Notebook is 20 cm long. (b) Detail of Type 1 magnesite veinlets with 'lettuce leaf' morphology from upper part of Fig. 7a. Finger is 6 cm long.

Fig. 8. SEM images of: (a) tabular, euhedral hydromagnesite crystals, and (b) hexagonal, platy, pyroaurite micro-crystals developed on hydromagnesite blades. Samples from LS-1 and 2 in Fig. 1).

Fig. 9. Cross plot of stable carbon and oxygen isotope data isotope from Mg-(hydro) carbonates, showing fields for equilibrium Mg-(hydro) carbonates precipitating from likely fluid end-members (blue boxes) based on Deines (2008)

for carbon and the H_2O-magnesite oxygen isotope relationship calibrated with dolomite data (Aharon 1988). The Soussaki field accommodates possible fluid $\delta^{18}O$ from +2‰ (= +29 ‰ carbonate) to -1‰. Red dots represent Type 2 vein-type magnesites in ultramafics and Neogene marl (M). The other symbols represent Type 1 near surface crusts, cotton balls and veinlets. Dots = magnesite, open circles = hydromagnesite and triangles = huntite. Orange colours are samples close to the volcanic centre (LS-6, 7 and 8; Fig. 1), blue colours represent samples km's from the volcanic centre (LS-5; Fig. 1) and green colours represent samples >10 km from the volcanic centre (N study area, LS1, 2 and 3; Fig. 1). The field ($\pm 1\sigma$) for local calcretes are from Table 4.

Table 1. Mineralogical and stable isotope data for various Mg-(hydro) carbonates hosted in altered ultramafics (unless specified otherwise) with sample context, trace mineralogy and proximity to volcanic centre. LS sample localities are shown on Fig. 1, except Ag Theod (Agio Theodoroi) which is a small and isolated serpentinite outcrop about 5.5 km E of LS-6 (Fig. 1). D, dolomite, S, serpentine. Where replicate and triplicate variability significantly exceed analytical precision they likely indicate natural heterogeneity.

Table 2. Indicative EMPA data for the main discrete mineral phases discussed in this study. Analysis for Na, K and Co were below detection (bd) in all minerals. LS sample localities are shown on Fig. 1.

Table 3. Geochemical data for water samples and contextual published data. LS sample localities are shown on Fig. 1. Note that one sample from Mavro (Mavro Limni) waterfall (*) returned reproducible, but unusually heavy isotopic compositions. We cannot explain these values and conclude that the isotope sample was probably compromised in some way. For this reason the values are excluded from calculations of area means or detailed discussion. Precision at 1σ were ±0.15‰ for $\delta^{18}O$ and ±2‰ for $\delta^{2}H$. Mean Soussaki groundwater data from Kelepertsis et al. (2001) where T ranges (*) between 40-21 ˚C. Mean N. Peloponnese spring water values from unpublished data of J.E. Andrews.

Table 4. Summary statistics of stable isotope compositions of local modern-late Pleistocene palaeosol calcites measured by J. E. Andrews and from Brasier (2007).

Table 1

Sample ID	Sample context/mineralogy	trace minerals	$\delta^{13}C$ ‰ VPDB	$\delta^{18}O$ ‰ VPDB	$\delta^{18}O$ ‰ VSMOW
***Type 1*: Near surface crusts, veinlets, cotton balls**					
Close to volcanic centre					
s107cwc	LS-8, magnesite	S	1.1	-0.6	30.3
s107k	LS-8, magnesite		-0.4	-1.8	29.1
s107xw	LS-8, magnesite		-13.4	-0.6	30.3
s10-7cw3	LS-8, magnesite & hydromagnesite	S	0.1	-1.9	29
s107Nnd	LS-8, hydromagnesite	S	-1.9	-1.6	29.3
AG-TH-12A	LS-6, huntite		-4.4±0.08(3)	-3.6±0.9(3)	27.2±0.9(3)
AG-TH-12B	LS-6, huntite		-4.0±0.5(3)	-2.9±1.0(3)	27.9±1.0(3)
AG-TH-12C	LS-6, huntite		-4.3±0.3(3)	-3.2±0.6(3)	27.6±0.6(3)
s107 aw	LS-8, huntite	S	2.0	-1.8	29.1
s107blt	LS-8, huntite		-0.1	-1.5	29.3
South study area, kms from volcanic centre					
smga	Ag. Theod, magnesite	D	6.6	-5.4	25.4
s-sc	Ag. Theod, magnesite		-13.4	-0.6	30.3
AG-TH-1	LS-6, magnesite vein		-5.5	-2.7	28.1
SOUS-2-UP	Ag. Theod, magnesite		-13.9±0.5(2)	-1.5±0.8(2)	29.4±0.8(2)
SOUS-1-SZA	Ag. Theod, magnesite		-2.7±0.2(2)	-1.4±0.7(2)	29.5±0.7(2)
am4fcl	LS-5, magnesite, cauliflower		-4.9	-1.9	29.0
amwvsi	LS-6, magnesite vein	S	-10.1	-1.5	29.4

	ath31h	LS-6, magnesite & huntite	S	-4.0	-2.6	28.2
	ath31	LS-6, huntite & magnesite	S	-3.4	-3.3	27.5
	am29	LS-6, huntite	S	-4.5	-3.0	27.8
	AG-TH-4-11	hydromagnesite		-14.4±0.2(2)	-1.0±0.3(2)	29.9±0.3(2)
North study area, >10kms from volcanic centre						
	ALPX-2	LS-2, magnesite, hard-crust		-10.3±0.4(3)	-1.9±0.7(3)	28.9±0.7(3)
	al2cf	LS-2, magnesite		-10.3	-1.4	29.5
	mF1F	LS-3, magnesite		5.6	-6.4	24.3
	mpf2cl	LS-1, hydromagnesite, cauliflower		-11.6	-0.8	30.1
	ALEPO-2	LS-2, hydromagnesite		-12.0±0.05(2)	-0.9±0.07(2)	30.0±0.07(2)
	ALEPO-4	LS-2, hydromagnesite nodule		-14.3±0.05(2)	-1.3±0.2(2)	29.6±0.2(2)
	ALEPO-6	LS-2, hydromagnesite crust		-14.9±0.6(3)	-1.2±0.2(3)	29.7±0.2(3)
	ALPX-1A	LS-2, hydromagnesite		-14.0±0.3(2)	-1.0±0.01(2)	29.9±0.01(2)
	f2b	LS-3, hydromagnesite		-9.14	-2.2	28.64
***Type 2*: Vein magnesites**						
	1	LS-6 in ultramafics		-9.8	-3.2	27.7
	10	LS-5, in ultramafics		-9.0	-3.2	27.6
	11	LS-6 in ultramafics		-9.7	-2.7	28.1
	s-plc	LS-7, in Neogene marl		7.3	-2.8	28.1
	ad4v	LS-7, in Neogene marl	D	3.8	-5.1	25.7

Table 2

	Hydromagnesite		**Magnesite**	**Dolomite**	**Pyroaurite**		**Serpentine**
	FAN-2 (LS-3)	*MP-1-B2 (LS-1)*	*AGTH31 (LS-6)*	*AGTH31*	*PRAE-3(LS-1)*	*MP-1-B2 (LS-1)*	*PRAE-3 & MP-1-B2*
	(n=2)	*(n=2)*	*(n=3)*	*(n=4)*	*(n=3)*	*(n=2)*	*(n=2)*
MgO	42.0	42.0	42.9	23.3	34.4	33.5	41.6
Al_2O_3	0.2	0.1	bd	bd	bd	0.2	0.4
SiO_2	0.2	0.1	0.1	0.2	0.1	0.1	41.6
CaO	0.0	0.1	2.5	26.7	0.1	0.2	0.1
Cr_2O_3	bd	bd	bd	bd	bd	bd	0.1
MnO	bd	bd	0.1	0.1	bd	bd	bd
NiO	bd	bd	bd	bd	1.8	2.2	0.2
FeO	bd	nd	0.2	0.3	bd	bd	bd
Fe_2O_3	0.1	0.1	bd	bd	24.6	24.1	3.8
Total	**42.5**	**42.4**	**45.8**	**50.6**	**60.9**	**60.3**	**87.8**

Table 3

		Conductivity ($\mu S\ cm^{-1}$)	TDS ($mg\ L^{-1}$)	pH	Eh (mV)	T (°C)	Ca^{2+} ($mg\ L^{-1}$)	Mg^{2+} ($mg\ L^{-1}$)	HCO_3^- ($mg\ L^{-1}$)	SO_4^{2-} ($mg\ L^{-1}$)	Cl^- ($mg\ L^{-1}$)	Mg/Ca (element ratio)	molar Mg/Ca	δ^2H ‰ VSMOW	$\delta^{18}O$ ‰ VSMOW
North coast	**LS 1 area**														
	Mavro Waterfall (1)*	1098	605	8.6	-110	21.4	3.0	120	558	15.0	38	40	66	-17	-4.6
	Mavro, Waterfall (2)	1020	520	8.6	-103	20.2	2.8	154	578	15.6	43	55	91	-37	-6.6
	Mavro, Pipes (1)	680	340	9.3	-142	19.4	0.8	89	354	2.1	31	111	183	-23	-6.7
	Mavro, Pipes (2)													-36	-6.4
	Schinos fountain	680	341	9	-124	20	1.2	87	371	0.3	28	72	180	-33	-7.5
Gerania Mountains LS-3 and 4 area															
	Sorovica spring, LS-3	540	270	8.65	-106	19.7					16			-30	-7.1
	Liaki spring													-41	-6.9
	Panagia-Faneromeni spring													-44	-7.4
	Gouro spring													-35	-8.3
Soussaki geothermal water LS-8 area															
	Soussaki (1)													-33	-5.4
	Soussaki (2)													-32	-5.3
	Mean Soussaki groundwater (Kelepertsis et al., 2001)			7.2		29	133	280		262	4299	2.1	3.5	-29	-4.3
	Mean tufa precipitating springwater N. Peloponnese (n=4)			8.1		16.5	81	17	217			0.2	0.4		-8.4

Table 4

	MEAN	MIN.	MAX.	STD. DEV.
δ^{13}C ‰ VPDB	-8.7	-10.2	-7.1	0.76
δ^{18}O ‰ VSMOW	+24.9	+21.44	+27.44	1.33

Fig 1a

Click here to download Figure Fig. 1a new.eps

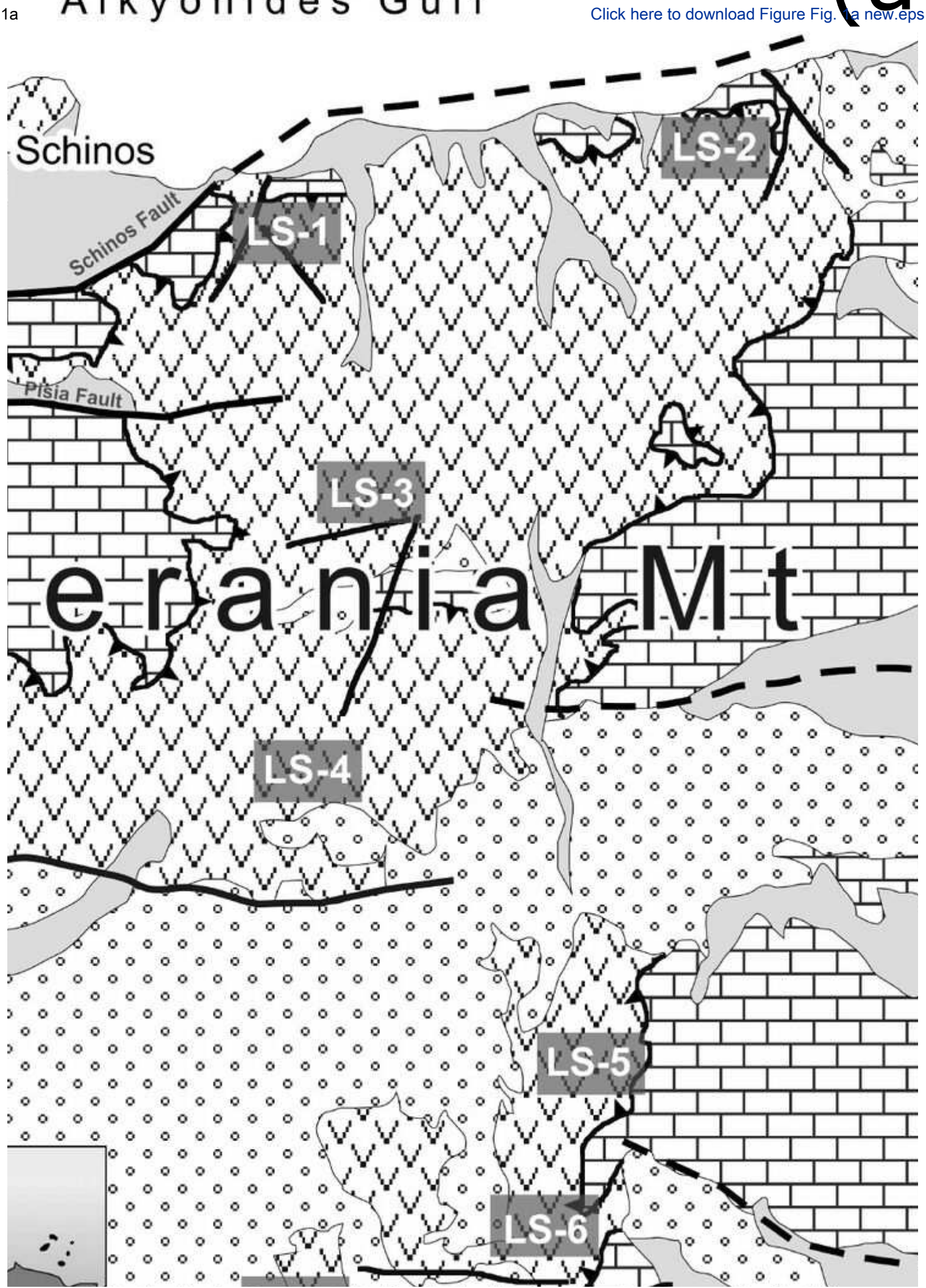

Fig 1b

Click here to download Figure Fig. 1b section.eps

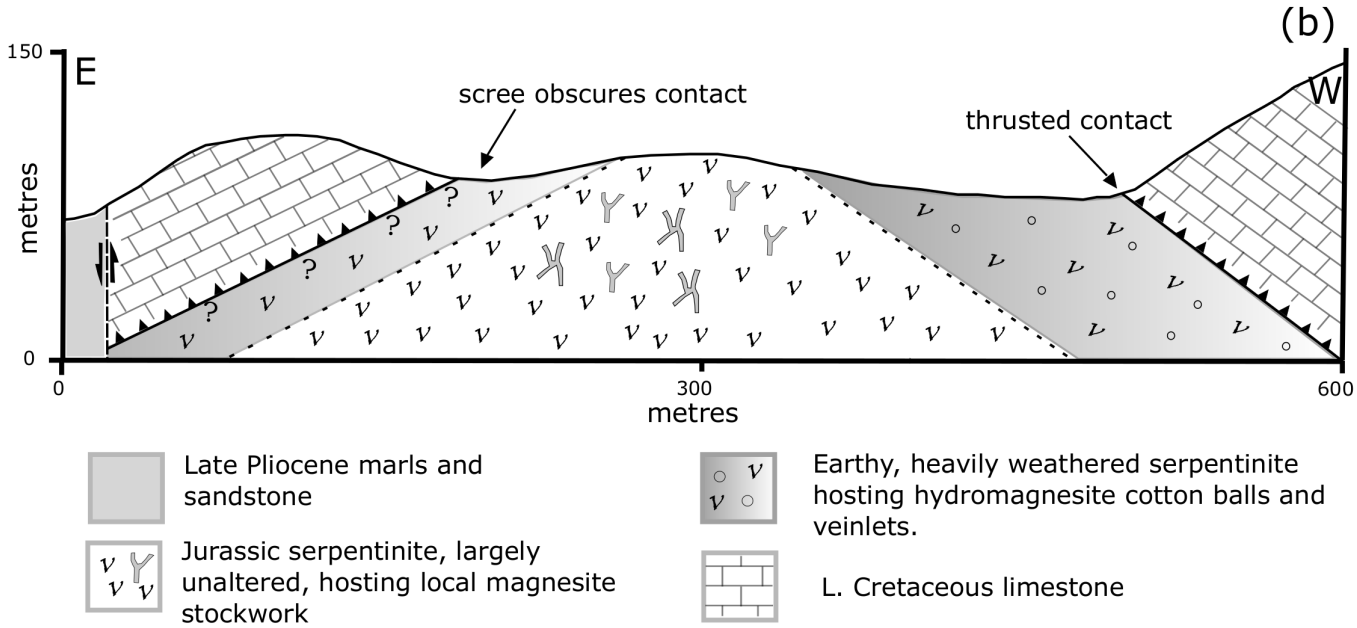

Fig 2

Click here to download Figure Fig. 2.tif

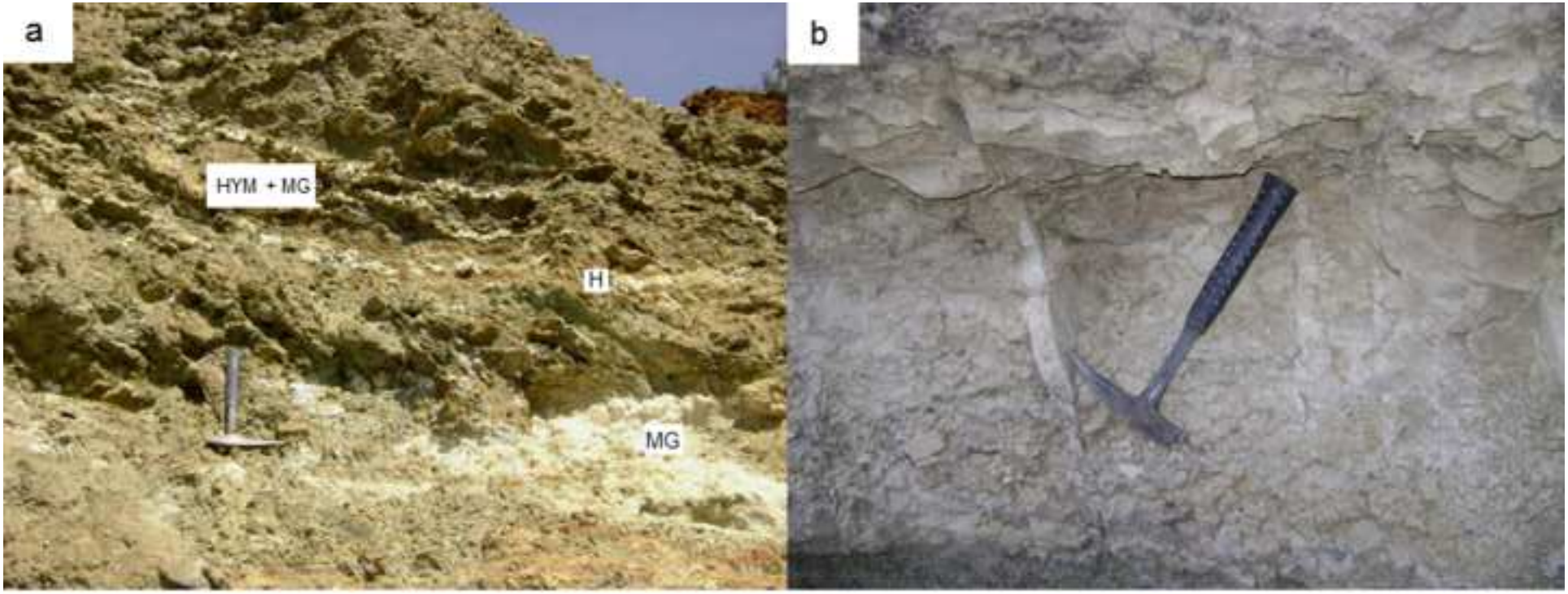

Fig 3a

Click here to download Figure Fig. 3a.tif

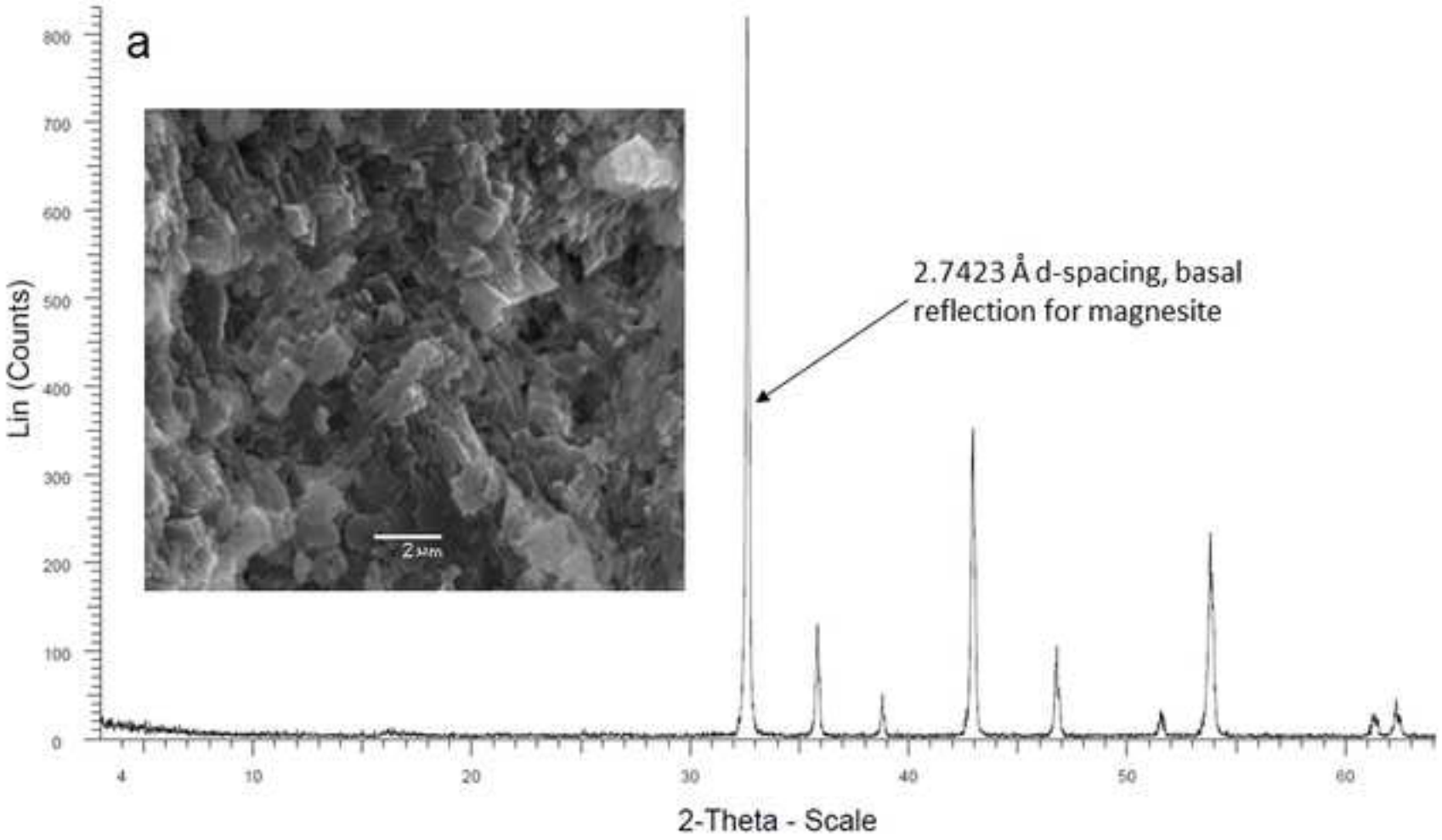

Fig 3b

Click here to download Figure Fig. 3b.tif

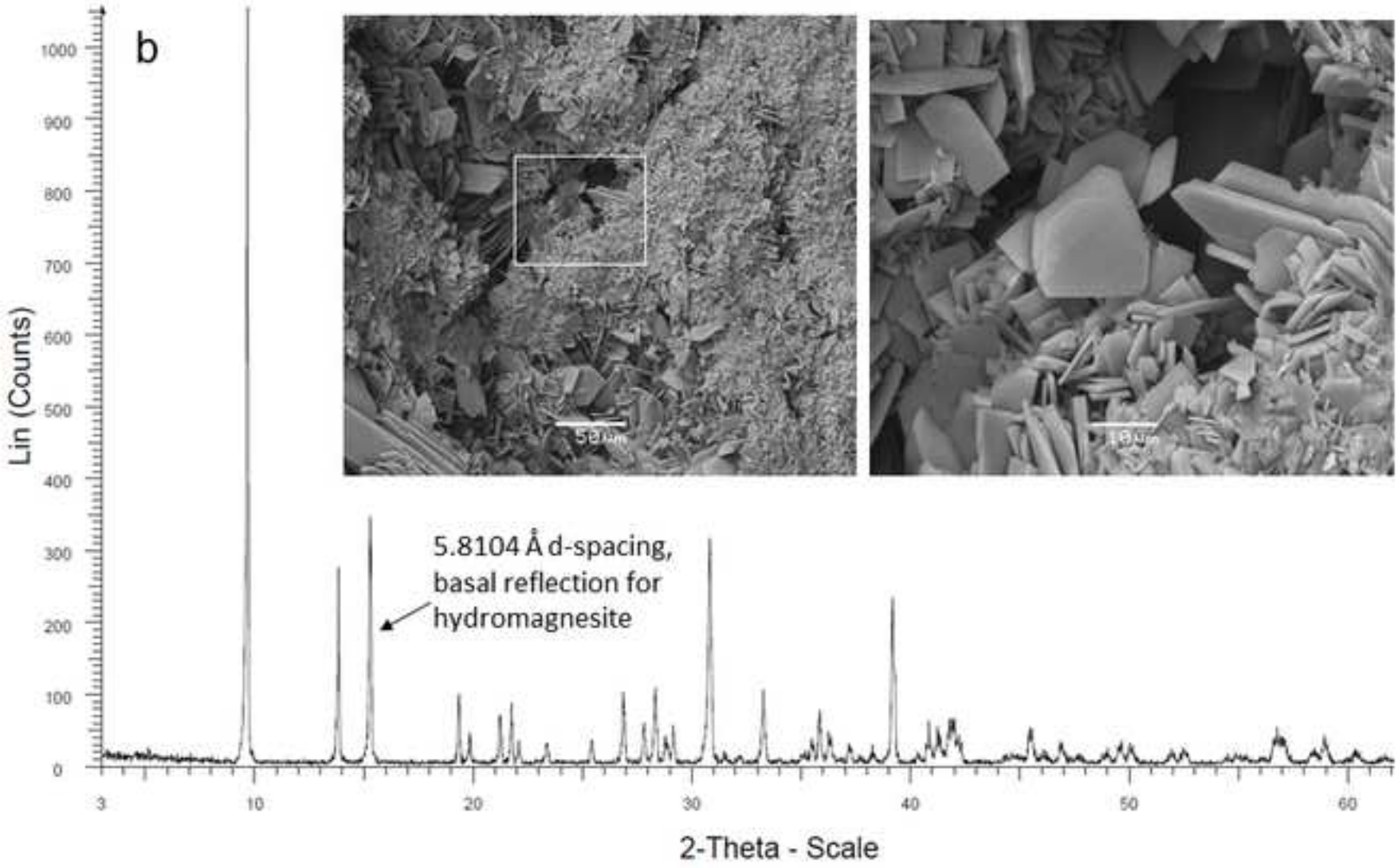

Fig 3c

Click here to download Figure Fig. 3c.tif

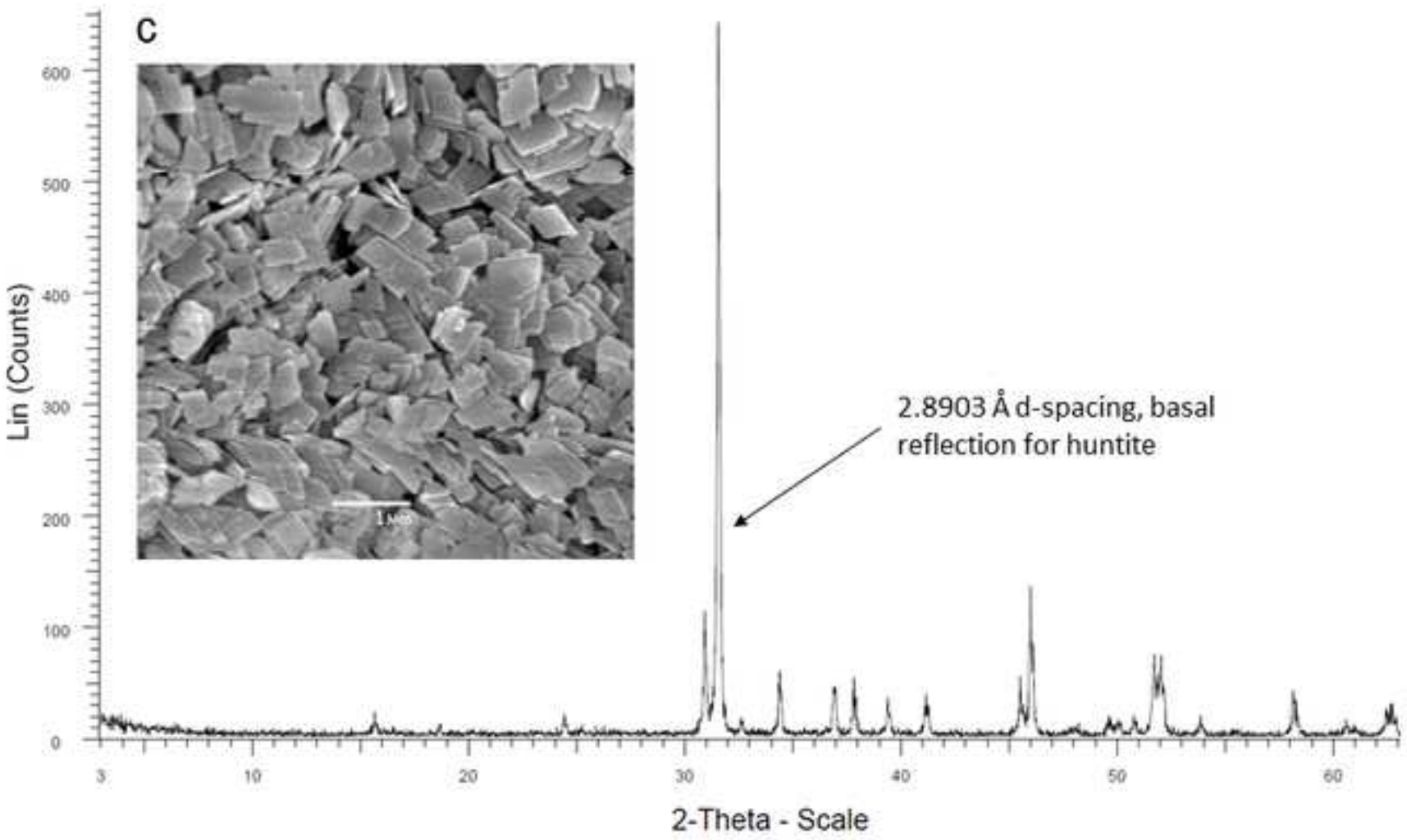

Fig 4

Click here to download Figure Fig. 4 revised.tif

Fig 5

Click here to download Figure Fig. 5.tif

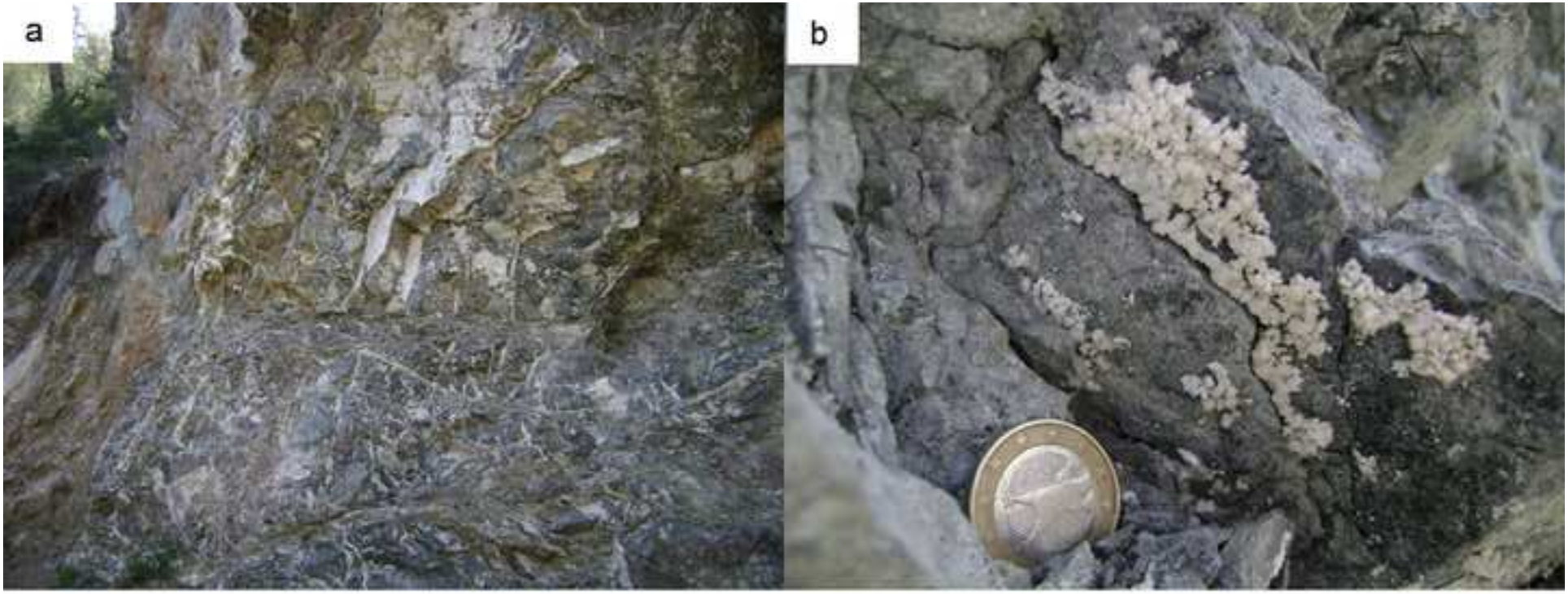

Fig 6

Click here to download Figure Fig. 6.tif

Fig 7

Click here to download Figure Fig. 7.tif

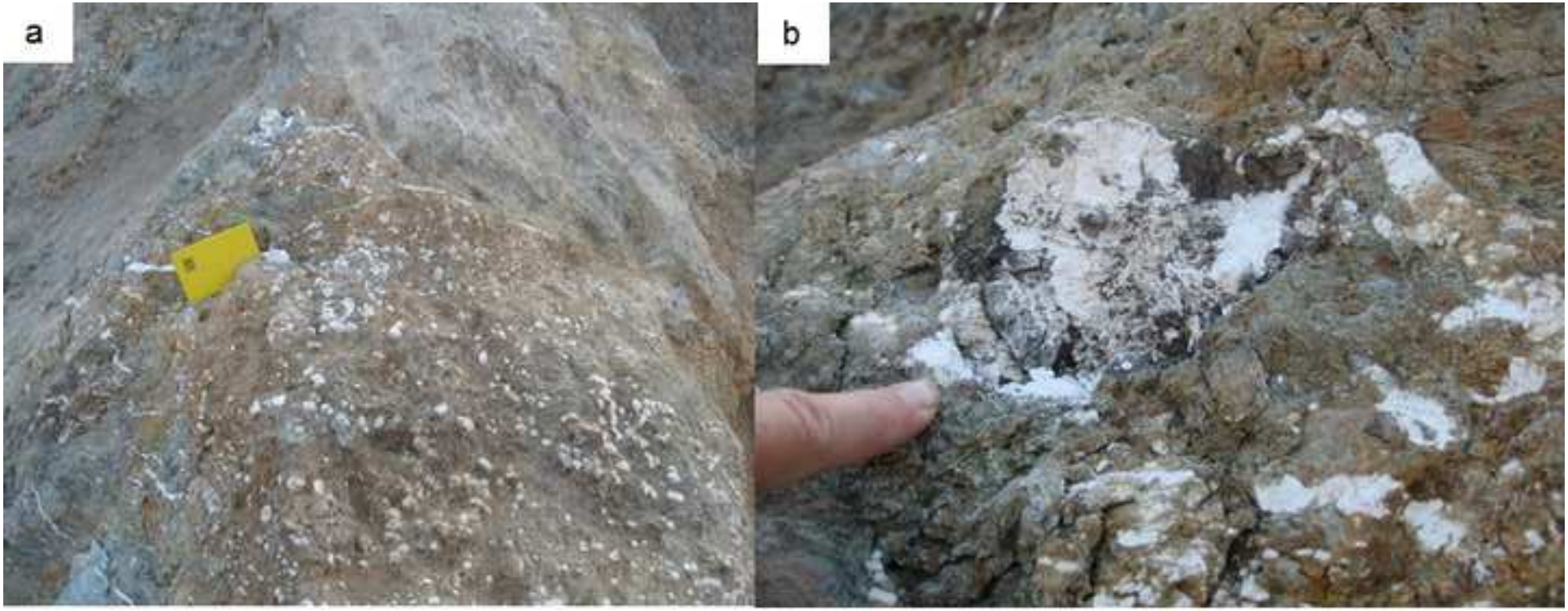

Fig 8

Click here to download Figure Fig. 8 new.tif

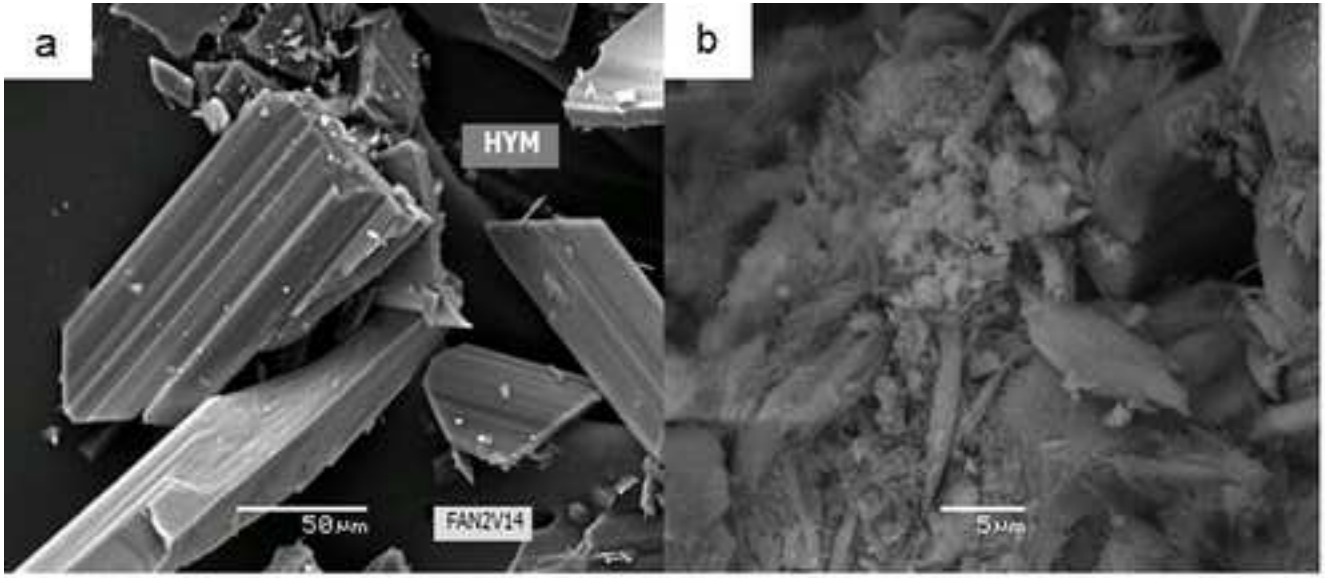

Fig 9

Click here to download Figure Fig. 9 revised 2017.tif